© 2022. Published by The Company of Biologists Ltd | Development (2022) 149, dev199944. doi:10.1242/dev.199944

RESEARCH ARTICLE

Female meiosis II and pronuclear fusion require the microtubule transport factor Bicaudal D

Paula Vazquez-Pianzola[1,*], Dirk Beuchle[1], Gabriella Saro[1], Greco Hernández[2], Giovanna Maldonado[2], Dominique Brunßen[1], Peter Meister[1] and Beat Suter[1,*]

ABSTRACT

Bicaudal D (BicD) is a dynein adaptor that transports different cargoes along microtubules. Reducing the activity of BicD specifically in freshly laid *Drosophila* eggs by acute protein degradation revealed that BicD is needed to produce normal female meiosis II products, to prevent female meiotic products from re-entering the cell cycle, and for pronuclear fusion. Given that BicD is required to localize the spindle assembly checkpoint (SAC) components Mad2 and BubR1 to the female meiotic products, it appears that BicD functions to localize these components to control metaphase arrest of polar bodies. BicD interacts with Clathrin heavy chain (Chc), and both proteins localize to centrosomes, mitotic spindles and the tandem spindles during female meiosis II. Furthermore, BicD is required to localize clathrin and the microtubule-stabilizing factors transforming acidic coiled-coil protein (D-TACC/Tacc) and Mini spindles (Msps) correctly to the meiosis II spindles, suggesting that failure to localize these proteins may perturb SAC function. Furthermore, immediately after the establishment of the female pronucleus, *D-TACC* and *Caenorhabditis elegans BicD*, *tacc* and *Chc* are also needed for pronuclear fusion, suggesting that the underlying mechanism might be more widely used across species.

KEY WORDS: *Drosophila* meiosis, Mitosis, Spindle assembly, Clathrin, Bicaudal D, BicD, TACC, CH-TOG, Microtubule transport, DeGradFP

INTRODUCTION

Encoded by a single gene, the *Drosophila* Bicaudal D (BicD) protein is part of a family of evolutionarily conserved dynein adaptors responsible for the transport of different cargoes along microtubules (MTs) (Vazquez-Pianzola et al., 2016; Hoogenraad and Akhmanova, 2016; Vazquez-Pianzola and Suter, 2012). The founding member of this protein family, *Drosophila* BicD, was identified because of its essential role during oogenesis and embryo development, in which it transports mRNAs that control polarity and cell fate (Bullock and Ish-Horowicz, 2001; Suter and Steward, 1991; Suter et al., 1989; Wharton and Struhl, 1989). This process is mediated by its binding to the RNA-binding protein Egalitarian (Egl) (Dienstbier et al., 2009; Mach and Lehmann, 1997). Since its initial discovery, BicD and its orthologs have been shown to control a diverse group of MT transport processes through binding to different cargoes or adaptor proteins (Hoogenraad and Akhmanova, 2016; Vazquez-Pianzola and Suter, 2012).

BicD can alternatively bind to Clathrin heavy chain (Chc) and this interaction facilitates Chc transport of recycling vesicles at the neuromuscular junctions and regulates endocytosis and the assembly of the pole plasm during oogenesis (Li et al., 2010; Vazquez-Pianzola et al., 2014). The best-known function of Chc is in receptor-mediated endocytosis, in which it forms part of clathrin, a trimeric scaffold protein (called a triskelion), composed of three Chc and three Clathrin light chains (Clc) (Brodsky, 2012). Aside from this, clathrin was shown to localize to mitotic spindles in mammalian and *Xenopus* cells (Fu et al., 2010; Royle et al., 2005) and to have non-canonical activity by stabilizing the spindle MTs during mitosis (Royle, 2012). This function depends on clathrin trimerization and its interaction with Aurora A-phosphorylated Transforming Acidic Coiled-Coil protein 3 (TACC3) and the protein product of the colonic hepatic Tumor Overexpressed Gene (ch-TOG) (Booth et al., 2011; Fu et al., 2010; Lin et al., 2010; Royle and Lagnado, 2006; Royle et al., 2005). This heterotrimer forms intermicrotubule bridges between kinetochore fibers (K-fibers), stabilizing these fibers and promoting chromosome congression (Booth et al., 2011; Royle et al., 2005). More recently, TACC3 and a mammalian homolog of Chc (CHC17) were shown to control the formation of a new liquid-like spindle domain (LISD) that promotes the assembly of acentrosomal mammalian oocyte spindles (So et al., 2019).

In order to transport its cargos along MTs, BicD interacts with the dynein/dynactin motor complex, a minus-end-directed MT motor. This complex is involved in different cellular processes, including intracellular trafficking of proteins and RNAs, organelle positioning and microtubule organization, some of which also require BicD. The dynein/dynactin complex also plays essential roles during cell division, in which it is required for centrosome separation, chromosome movements, spindle organization and positioning and mitotic checkpoint silencing (Raaijmakers and Medema, 2014).

Given that *Drosophila* BicD forms complexes with Chc and Dynein, both of which, as described above, perform essential activities during mitosis, we set out to investigate possible *BicD* functions during cell division. Reducing BicD levels by specific protein-targeted degradation in freshly laid eggs revealed that BicD is essential for pronuclear fusion. In addition, it is required for metaphase arrest of female meiotic products after meiosis II completion. This activity appears to be mediated by the role of BicD in localizing the spindle assembly checkpoint (SAC) components. Furthermore, BicD interacts with its cargo protein, Chc, and they both localize to the mitotic spindles and centrosomes and the female tandem meiotic II spindles. In addition, BicD localizes D-TACC, clathrin, and Mini spindles (Msps; ch-TOG homolog) to the meiosis II spindles. The failure to localize these proteins accurately might

[1]Institute of Cell Biology, University of Bern, 3012 Berne, Switzerland. [2]Laboratory of Translation and Cancer, Unit of Biomedical Research on Cancer, Instituto Nacional de Cancerología (INCan), 14080-Tlalpan, Mexico City, Mexico.

*Authors for correspondence (beat.suter@unibe.ch; paula.vazquez@unibe.ch)

P.V.-P., 0000-0002-4275-8966; P.M., 0000-0002-6230-4216

Handling Editor: Thomas Lecuit
Received 1 July 2021; Accepted 25 May 2022

Development (2022) 149, dev199944. doi:10.1242/dev.199944

also contribute to the SAC function defects observed in embryos with reduced BicD levels. D-TACC and *Caenorhabditis elegans bicd-1*, *tac-1* and *chc-1* are also needed after fertilization for pronuclear fusion, revealing an evolutionary conserved and essential role of these proteins in early zygote formation and suggesting that their mechanism of action on MTs might be widely used across species.

RESULTS

BicD and its cargo clathrin localize to centrosomes and spindles during mitosis and tandem spindles in meiosis II

Completion of female meiosis and the first mitotic cycles depend on correct spindle formation in the egg and the developing embryo. Inactivation of maternally expressed genes, which provide all the proteins that control these first divisions, leads to either maternal effect lethality or female sterility. Indeed, *BicD* loss-of-function mutants are female sterile because they do not produce oocytes (Ran et al., 1994), which is an obstacle to studying the role of *BicD* in maternally controlled early embryonic mitotic divisions. Our laboratory has developed $BicD^{mom}$ females, a method to overcome *BicD* mutant female sterility (Swan and Suter, 1996). $BicD^{mom}$ females provide *BicD* from an inducible promoter that can be turned off once oocyte fate is established. Around 3-to-4 days after shutting down *BicD*, $BicD^{mom}$ ovaries contain egg chambers devoid of BicD, and few of these chambers develop into eggs (Swan and Suter, 1996; Vazquez-Pianzola et al., 2014). Using this strategy, we observed that the eggs laid by $BicD^{mom}$ females did not develop but were arrested during stage 1 of embryonic development with phenotypes that required a more detailed analysis (see below) (Fig. S1A; Movies 1-4). These results suggest that *BicD* is also essential downstream of oocyte differentiation to complete meiosis and progress through the early mitotic divisions.

We analyzed BicD localization during mitosis in methanol-fixed embryos. Methanol fixation dissolves the cytosolic pool of BicD, making insoluble pools of the protein more apparent. Surprisingly, during the syncytial divisions, BicD was detected on the centrosomes, where it colocalized with the pericentrosomal marker centrosomin (Cnn) and along the mitotic spindles (Fig. 1A,a,b; Fig. S1B). During cellularization, BicD was additionally enriched at the plasma membrane (Fig. 1Ac). We additionally analyzed embryos expressing BicD::GFP. Both methanol and GFP staining patterns were highly similar (Fig. S1C), confirming the specificity of the BicD antibodies.

The first spindles observed in freshly laid eggs are the female meiotic II tandem spindles. However, assessing BicD localization in these eggs was challenging because of the high levels of BicD in the cytoplasm. A specific BicD signal was observed using anti-BicD antibodies, but its level was the same in the meiotic spindle region as in the cytoplasm (Fig. S1D). Anti-GFP antibodies in *BicD::GFP,* $BicD^{null}$ eggs detected the presence of BicD at the meiotic spindle more clearly. BicD::GFP was enriched above cytoplasmic levels on the meiotic tandem spindles and the central aster (Fig. 1B,B′; Fig. S1E).

Thus, we conclude that BicD associates with the mitotic spindles and the centrosomal region during mitosis and with the tandem spindles and the central aster during female meiosis II. Given that mammalian BicD1 and BicD2 are present at the centrosomes in mammalian cells (Fumoto et al., 2006), our data suggest that *BicD*

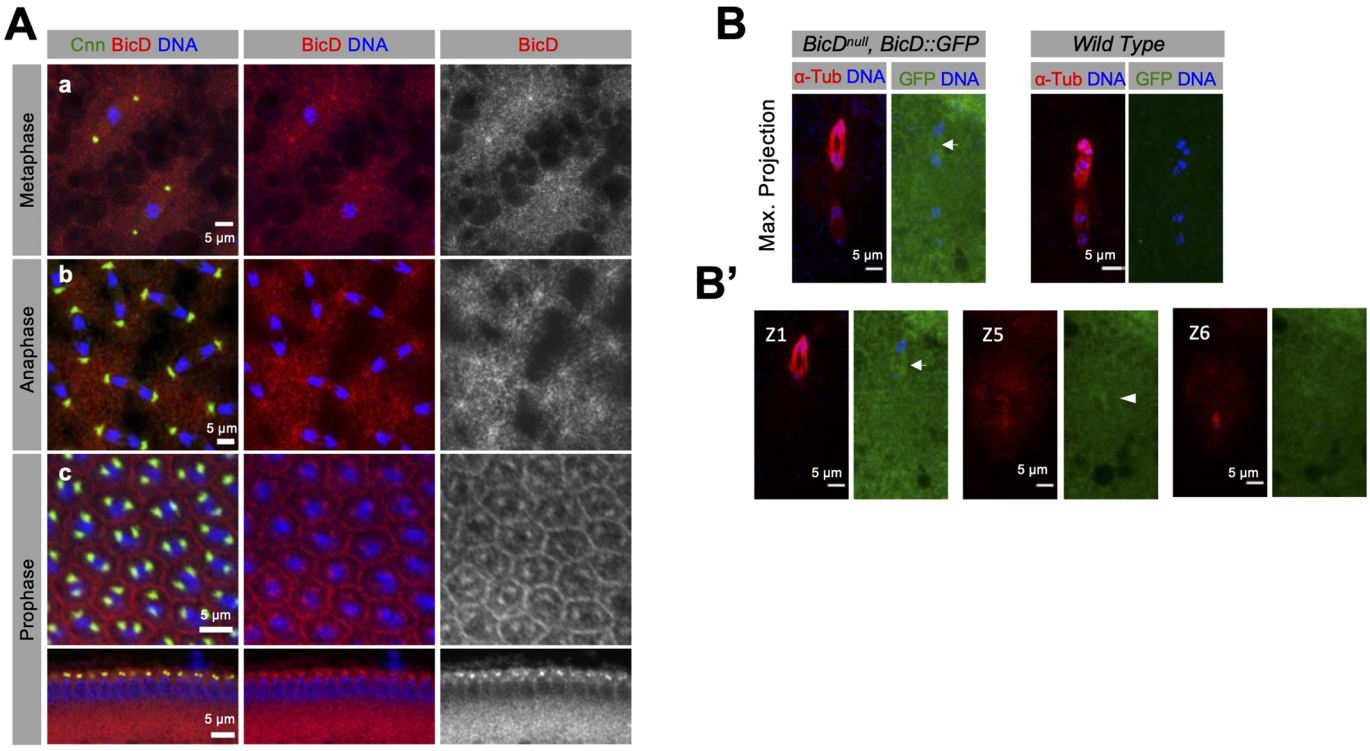

Fig. 1. BicD localizes to mitotic spindles and centrosomes, and the female MII spindles. (A) BicD (red) is present at metaphase spindles and colocalizes with the pericentrosomal marker Cnn (green). Wild-type embryos in nuclear cycle 10 (NC10) (a), NC12 (b) and during cellularization (NC14) (c). (B,B′) An all tandem spindle. BicD::GFP (detected with anti-GFP antibodies) is enriched in the region of the tandem spindles (arrows indicate the most superficial spindle) and the central aster (arrowhead) above cytoplasmic levels. Embryos were also stained for α-tubulin (red). Enrichment at the most superficial spindle is only detected in the maximum projection image because of the high cytoplasmic levels of BicD::GFP in the upper frames. The BicD::GFP signal at the central aster (arrowhead) becomes more evident when the deeper *Z*-planes are analyzed (B′; see *Z*5 and *Z*6 images). Hoechst 33258 (blue) was used to stain the DNA in all embryos.

Development (2022) 149, dev199944. doi:10.1242/dev.199944

might play a currently unidentified but evolutionarily conserved role at the mitotic/meiotic spindles.

deGradFP knockdown of BicD::GFP reveals a previously unknown essential role for BicD during early embryogenesis

The number of eggs laid by *BicD*^{mom} flies was too small for phenotypic analyses. Thus, we designed a strategy to knock down BicD directly in young embryos (stage 1) using the degrade GFP (deGradFP) technique, a method to target GFP-fusion proteins for destruction or inactivation (Caussinus et al., 2011). We took advantage of the functional genomic *BicD::GFP* construct (Paré and Suter, 2000) and also constructed a deGradFP system specifically active during embryogenesis but not during oogenesis. We expressed the deGradFP (NSlmb-VhhGFP4) from a *hunchback* (*hb*) minimal maternal promoter coupled with the *bicoid* (*bcd*) 3′-untranslated region (UTR) (Fig. 2A). The *hb* promoter is active during late oogenesis; thus, the *deGradFP* mRNA will be loaded into eggs and embryos (Fig. 2A′). The *bcd* 3′-UTR promotes mRNA localization to the anterior pole of the oocyte and egg. It also allows translation only upon egg activation in freshly laid eggs, which occurs when metaphase I (MI) Stage (S) 14 egg chambers pass through the oviduct (Berleth et al., 1988; Driever and Nüsslein-Volhard, 1988; Sallés et al., 1994). We refer to this construct as *hb-deGradFP*. We corroborated the enrichment of the *deGradFP* mRNA in the anterior region of the embryo from egg laying until before cellularization (Fig. 2B). Immunostaining experiments to detect *hb-deGradFP* expression revealed that Vhh-GFP was distributed throughout the embryo and did not form an anterior-posterior (A-P) gradient (Fig. 2C). Thus, deGradFP appeared to be stable and was able to move/diffuse to the rest of the embryo. Therefore, the *hb-deGradFP* tool should be useful to degrade GFP fusion proteins in entire young embryos.

BicD::GFP rescues the sterility phenotype and the embryonic developmental arrest of *BicD* loss-of-function mutants (*BicD::GFP, BicD*^{null} homozygous females) (Paré and Suter, 2000) (Fig. 2D,E). However, when these females expressed two copies of the *hb-deGradFP* construct (*BicD::GFP, BicD*^{null}; *hb-deGradFP* homozygous females), 75% of their progeny failed to develop into late embryonic stages and did not hatch into larvae. Instead, eggs and embryos arrested mainly in meiosis or the first mitotic divisions, as observed in embryos laid by *BicD*^{mom} females (Fig. 2D,E,H; Movies 5-7). Here, we refer to these progeny and their mothers as *BicD*$^{hb\text{-}deGradFP}$. Most embryos laid by females that expressed not only two copies of *hb-deGradFP*, but also a wild-type *BicD*$^{+}$ [*BicD::GFP, BicD*^{null}/+(CyO); *hb-deGradFP*], developed normally, indicating that high levels of *hb-deGradFP* expression on their own are not deleterious for development (Fig. 2D,E). *BicD*$^{hb\text{-}deGradFP}$ females had phenotypically wild-type ovaries that expressed normal BicD::GFP protein levels (Fig. 2F,G), confirming that the *hb-deGradFP* construct is not active during oogenesis. In contrast, in young *BicD*$^{hb\text{-}deGradFP}$ embryos, the BicD::GFP signal was reduced in the entire embryo (Fig. 2H) and BicD::GFP protein levels were downregulated by 50% (Fig. 2I). BicD::GFP is expressed at levels comparable to wild-type BicD (Fig. S2A). However, a 50% reduction in the levels of BicD::GFP detected by western blot produced already-visible phenotypes. In comparison, eggs from heterozygous females (*BicD*^{null}/+) that also had a 50% reduction of BicD compared with wild-type embryos (Fig. S2A) developed normally (97.3±1.03% embryos hatched into larvae). Although alternative explanations for these differences are possible, we suggest that deGradFP might bind BicD::GFP, functionally inactivating the protein before sending it for degradation.

As intended, deGradFP was highly expressed in young embryos, although low protein levels were detected in ovaries (Fig. 2G,I; Fig. S3A). Although we cannot rule out that some S14 oocytes were physically activated during dissection, it is also possible that the *bcd* 3′-UTR sequence was not sufficient to control translation fully in the context of the minimal maternal *hb* promoter and its 5′-UTR. Although BicD was also present at the MI spindles in S14 oocytes (Fig. S3B), *BicD*$^{hb\text{-}deGradFP}$ S14 oocytes displayed no evident problems in spindle formation or chromosome alignment in meiotic MI (Fig. S3C,D). This suggests that the early embryonic arrest observed in *BicD*$^{hb\text{-}deGradFP}$ individuals is not the result of earlier meiotic defects during late oogenesis.

BicD is required for the cell cycle arrest of male and the female meiotic products and for pronuclear fusion

To learn more about the previously unknown function of BicD during the earliest phase of embryonic development and to pinpoint the developmental stage in which BicD is active, we collected fully viable control embryos and *BicD*$^{hb\text{-}deGradFP}$ embryos over a 30 min period, let them develop for another 30 min (30-60 min-old collections) and analyzed them for developmental defects (Fig. 3A). Twenty-five minutes after eggs laying, control embryos finished the second mitotic division and contained at least four zygotic nuclei. At this early stage, normal zygotic nuclei reside in the interior of the embryo, and the three remaining female meiotic polar body products (mostly fused into one or two rosette-shaped nuclei) reside at the embryonic surface. Indeed, most embryos laid by control mothers [*BicD::GFP, BicD*^{null} or *BicD::GFP, BicD*^{null}/+(CyO); *hb-deGradFP*] developed normally, displaying more than four zygotic nuclei with wild-type-looking mitotic spindles (Fig. 3A,B). However, embryos laid by *BicD*$^{hb\text{-}deGradFP}$ mothers were arrested mainly at earlier developmental stages and displayed abnormal spindle-like structures (Fig. 3A,C). Even though they contained mainly centrally located dividing nuclei, around 25% of these embryos were classified as ‘arrested with centrosomes’ because they were stained positive for the centrosomal marker Cnn (Fig. 3A; example in Fig. 3Ca). In this category, we found embryos that contained at least one spindle displaying clear and sometimes fragmented staining for Cnn at the spindle poles. Additionally, they frequently displayed ‘free centrosomes’ marked by Cnn signals associated with α-tubulin but without a complete spindle and DNA (Fig. 3Ca1). Embryos showing acentrosomal spindles but containing free centrosomes were also scored into this category. Another 35% of the *BicD*$^{hb\text{-}deGradFP}$ embryos had one or more internal acentrosomal spindles that were negative for Cnn staining. These were classified as ‘arrested, acentrosomal’ (Fig. 3A,Cb).

Consistent with the fact that centrosomes are inherited from the father, embryos arrested and classified as ‘arrested with centrosomes’ were mostly marked by the presence of the sperm tail (Fig. S4A,B). In contrast, embryos displaying ‘acentrosomal’-like spindles and no free centrosomes rarely showed any of these sperm tail markers, indicating that they more likely represented unfertilized eggs with aberrant meiotic products (Fig. S4A,B). We then analyzed the phenotype of arrested fertilized *BicD*$^{hb\text{-}deGradFP}$ eggs in more detail by detecting the presence of the X and Y chromosomes. Male embryos (marked by the presence of the Y) develop only from fertilized eggs. Male embryos from control mothers showed one dot-like signal for the X chromosome and one signal for the Y chromosome in each zygotic nucleus, and these nuclei were in the interior of the embryo (Fig. 3D2). The three polar bodies, formed after two meiotic divisions, normally fused into a single polar body marked by the presence of the three

Development (2022) 149, dev199944. doi:10.1242/dev.199944

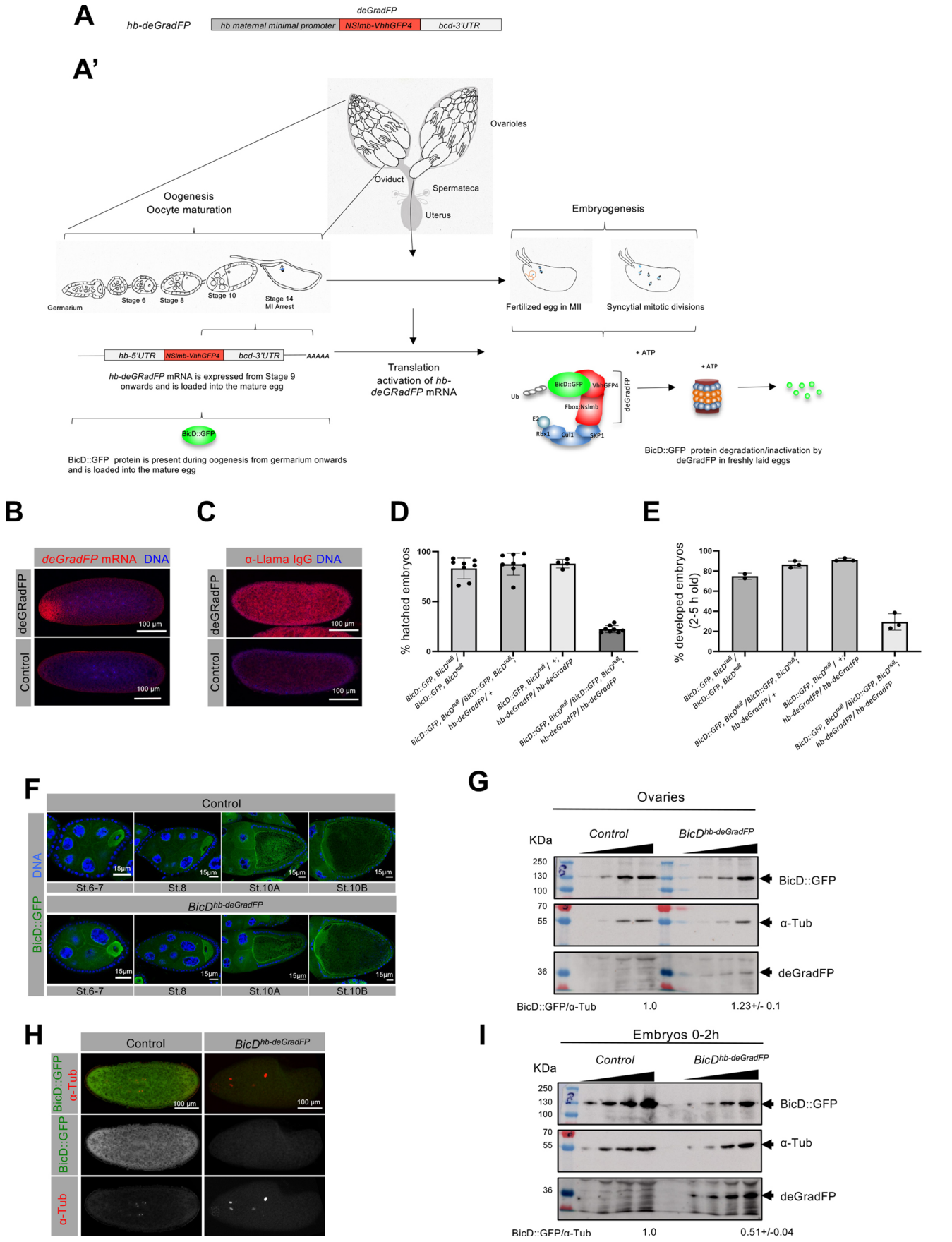

Fig. 2. See next page for legend.

Development (2022) 149, dev199944. doi:10.1242/dev.199944

Fig. 2. *hb-deGradFP* degrades BicD::GFP specifically in freshly laid eggs, causing early developmental arrest. (A) Schematic depicting the construct expressed in *Drosophila*. (A′) Model of the mechanism of action of the construct. (B) RNA FISH detection of *deGradFP* mRNA (red) enriched in the anterior region of freshly laid embryos. (C) The deGradFP construct (red signal) is ubiquitously present in young embryos. Wild-type embryos without the *deGradFP* transgene were used as negative controls in B and C. (D) Percentage of embryos of the depicted maternal genotype that hatched as larvae. (E) Percentage of normally developed embryos laid by mothers of the indicated genotypes. Data are means±s.d. (F-I) Ovaries and embryos produced from control (*BicD::GFP, BicD*^{null}) and *BicD*$^{hb\text{-}deGradFP}$ females. (F) BicD::GFP endogenous fluorescence signal (green) was detected in ovaries of different developmental stages (St.). (H) BicD::GFP in whole embryos was detected by using anti-GFP antibodies. Embryos were staged by anti-α-tubulin staining (red). (G,I) Western blots showing BicD::GFP and deGradFP levels in ovaries (G) and 0-2 h-old embryos (I). Increasing amounts of cytoplasmic extracts were loaded for each sample (α-tubulin was the loading control). The relative abundance of BicD::GFP/α-tubulin, normalized to the control, was calculated for the last two lanes. Hoechst 33258 (blue) was used to stain the DNA in all samples. deGradFP expression was detected using an anti-Llama serum that recognizes the Vhh GFP expressed from this construct.

X chromosomes (Fig. 3D1). In contrast, all arrested male embryos laid by *BicD*$^{hb\text{-}deGradFP}$ females had at least one internal spindle marked only by the presence of the Y chromosome, with no X chromosome signal (Fig. 3E-G). This pattern indicates that pronuclear fusion failed to occur and that a spindle still formed from the paternal pronucleus (Fig. 3E-G). In most of these embryos (70%), the male pronucleus underwent only one additional round of replication because two dots of the Y chromosome signal were observed in the internal metaphase spindle (Fig. 3E3). Embryos with more than one paternal spindle and many Y chromosome signals were also observed at a lower frequency (30%; Fig. 3F2,3,G4-6). Independent of the rounds of replication observed in the parental pronucleus, arrested *BicD*$^{hb\text{-}deGradFP}$ embryos also contained one or several acentrosomal nuclei marked frequently by several dots of X chromosomal signal (Fig. 3E1,2,F1,G1-4). This suggests that, in these *BicD*$^{hb\text{-}deGradFP}$ embryos, the female meiotic products did not arrest in metaphase II as they normally do but instead underwent several cycles of DNA replication instead. These results show that *BicD* is required for the cell cycle arrest of the female and male pronuclei and for pronuclear fusion. Similar phenotypes were observed in eggs laid by females in which *BicD* copies were further reduced by expressing a single copy of the *BicD::GFP* rescue construct (Fig. S5), suggesting that replication of the meiotic products can take place in the absence of most functional *BicD*. However, these females were unhealthy and died shortly after eclosing or during the first week after eclosion. During this time, they did not lay sufficient eggs for a complete phenotype analysis. Given that deGradFP only knocks down part of the BicD::GFP pool, the phenotypes observed in *BicD*$^{hb\text{-}deGradFP}$ embryos and analyzed in detail in this work are likely to resemble a hypomorphic rather than a null condition for *BicD*.

BicD is needed for replication arrest of the polar bodies and their rosette formation

To test for a direct role of *BicD* in female meiosis II, we crossed control and *BicD*$^{hb\text{-}deGradFP}$ females to sterile XO males, causing them to lay unfertilized eggs (Fig. 4). In unfertilized wild-type eggs, egg activation is triggered by passage through the oviduct, and this causes the eggs to complete meiosis II. We observed between one and four rosette-like nuclei in collections of unfertilized control eggs. These represent intermediate stages of the fusion process of the four meiotic products, which ultimately fused to form a single, rosette-shaped nucleus, indicating that eggs had completed meiosis II. These rosette-shaped nuclei were marked by a total of four dots of X-chromosomal signal per egg, which arise from each of the four meiotic products (Fig. 4A,B). In contrast, *BicD*$^{hb\text{-}deGradFP}$ unfertilized eggs contained one-to-several nuclei forming spindle-like structures, mostly with the appearance of multipolar spindles (Fig. 4A,C). Additionally, their chromosomes did not create the rosette structure that is typical of a metaphase-arrested state. Instead, these nuclei displayed partially decondensed chromatin, had an irregular shape and lacked the α-tubulin-staining ring seen surrounding the DNA rosette in control eggs (Fig. 4A,C). Furthermore, the X-chromosomal probe produced more than the usual four signal dots per egg in eggs containing only one meiotic product (Fig. 4Cc) and eggs containing several meiotic products and spindles (Fig. 4Cc′). We also observed eggs with more than four meiotic products (e.g. Fig. 4Cc′), indicating that *BicD*$^{hb\text{-}deGradFP}$ eggs show over-replication of meiotic products. The probe used for the fluorescence *in situ* hybridization (FISH) experiments recognizes a 359 bp repeat unit that spans several megabases on the X chromosome. The fact that this probe detected more than four signals in each *BicD*$^{hb\text{-}deGradFP}$ egg and that these signals showed different levels of brightness and size might also suggest that the DNA had become fragmented and/or more decondensed and did not arrest in a metaphase-like state as in the typical rosette structures. This replication, decondensation and/or fragmentation of the meiotic DNA was not restricted to the sex chromosomes because we observed analogously additional signals when using a probe for the second chromosome (Fig. S6). Altogether, these results indicate that BicD is required for both the replication arrest and formation of the typical rosette-like structures of the polar bodies.

Role of BicD in SAC and metaphase arrest of female meiotic products

After meiosis II completion, *Drosophila* polar bodies remain arrested in a metaphase-like state. In wild-type unfertilized eggs, the four meiotic products fused into a single rosette showed a strong signal for the mitotic marker Phospho-Histone 3 (PH3) along the entire chromosome, indicating that they were arrested in a metaphase-like state (Fig. 4Da-Ea). In contrast, in *BicD*$^{hb\text{-}deGradFP}$ eggs showing one rosette-like structure, indicative of meiosis completion, PH3 staining was not localized along the entire chromosomes but only enriched at the rosette central region, where most of the centromeres were observed (Fig. 4Db-Eb). Moreover, their rosette-like structures showed an increased number of CID-positive dots, suggesting that female meiotic products underwent extra rounds of replication/endoreplication (compare Fig. 4Da with Fig. 4Db).

Rosette-like structures in *BicD*$^{hb\text{-}deGradFP}$ eggs did not form the typical tubulin ring surrounding the chromosomes observed in wild-type eggs (Fig. 4E). Interestingly, DNA extended beyond this tubulin ring and was negative for PH3 staining (Fig. 4Ea,b,c1). In the wild-type situation, Histone H3 phosphorylation begins in pericentromeric heterochromatin regions at the onset of mitosis. It then spreads along the entire length of the chromosomal arms, reaching its maximal abundance during metaphase, followed by a rapid decrease upon transition to anaphase (Sawicka and Seiser, 2012). Thus, PH3 staining confined to the pericentromeric region in *BicD*$^{hb\text{-}deGradFP}$ polar bodies suggested that these nuclei were either not arrested appropriately or were released from metaphase arrest. Furthermore, *BicD*$^{hb\text{-}deGradFP}$ eggs having several meiotic products (Fig. 4Ec,c′) showed that not all these nuclei stained positive for PH3 (Fig. 4Ec2,c3,Ec′), further strengthening the idea that these nuclei were over-replicating because of a failure to arrest in metaphase.

Development (2022) 149, dev199944. doi:10.1242/dev.199944

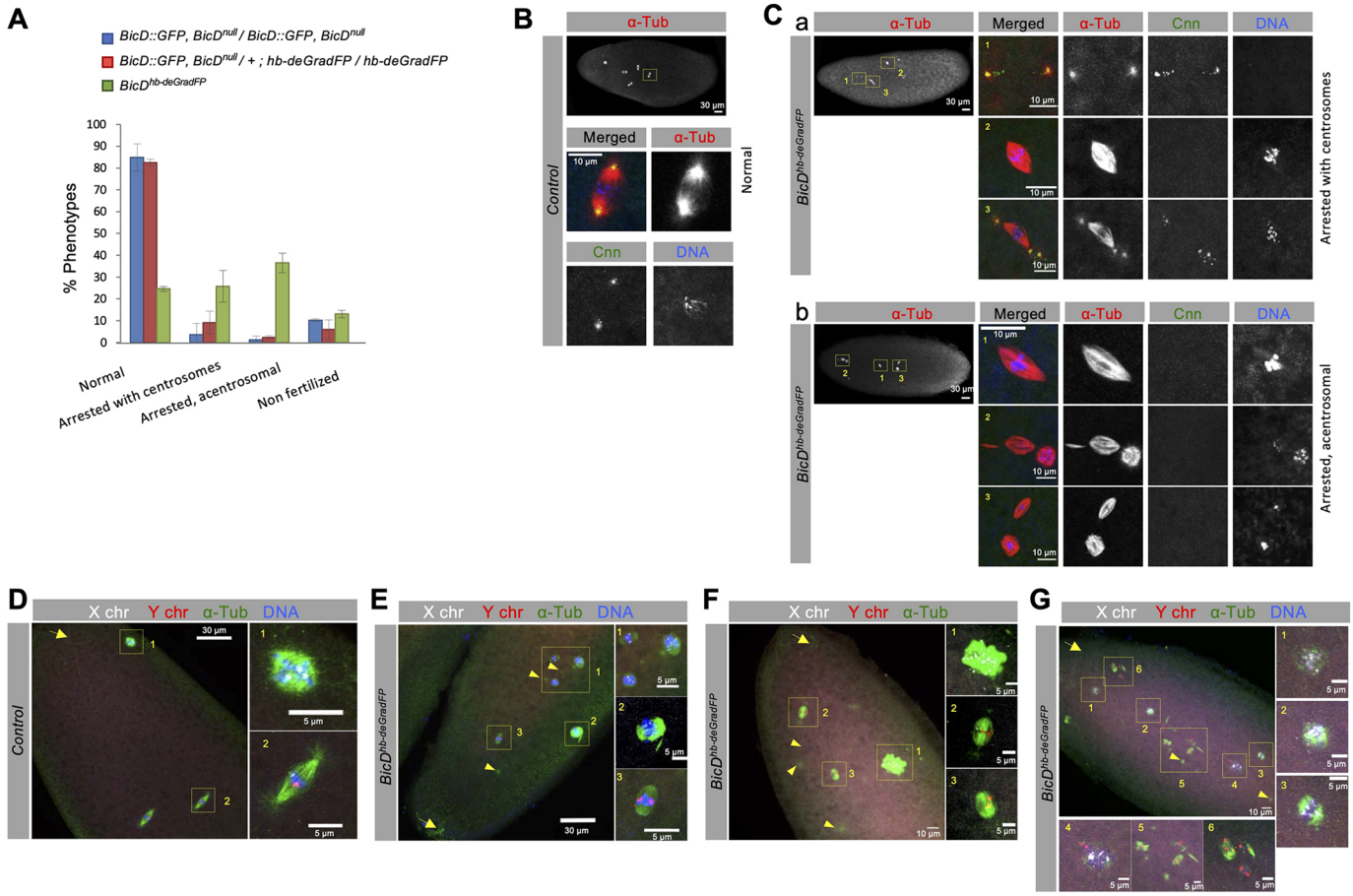

Fig. 3. Fertilized *BicD*$^{hb\text{-}deGradFP}$ embryos arrest at the start of embryogenesis with abnormal spindles, over-replicated female meiotic products and without pronuclear fusion. (A-C) 30-60 min-old embryos with the indicated maternal genotypes stained for α-tubulin (red), Cnn (green) and DNA (blue). (A) Percentage of embryos displaying the different phenotypes. The maternal genotypes are indicated. Embryos were characterized as unfertilized when no internal nuclei were seen and the four polar bodies, arranged in rosette-like structures (mostly fused into a single one), were observed at the surface of the embryo. Two independent collections (n1 and n2) were analyzed. Data are means±s.d. For *BicD::GFP, BicD*^{null}/*BicD::GFP, BicD*^{null} *n1*=84, *n2*=82; for *BicD::GFP, BicD*^{null}/*+; hb-deGradFP/hb-deGradFP n1*=55, *n2*=70; and, for *BicD*$^{hb\text{-}deGradFP}$, *n1*=42, *n2*=63. (B-C) Examples of the observed phenotypes. (B) Normal nuclear divisions in a control embryo (from a *BicD::GFP, BicD*^{null} mother). (C) Overview of the spindles seen in *BicD*$^{hb\text{-}deGradFP}$ embryos classified as either 'arrested with centrosomes' (a) or 'arrested, acentrosomal' (b). (D-G) DNA FISH with X (white) and Y (red) chromosomal probes and staining for α-tubulin (green) and DNA (blue). Arrows indicate the sperm tails and arrowheads indicate free centrosomes. (D) Example of a control wild-type male embryo in the second mitotic metaphase. (E-G) Examples of arrested *BicD*$^{hb\text{-}deGradFP}$ male embryos. Images are *Z*-stack projections through the nuclei; dashed-yellow boxes mark the corresponding magnified nuclei.

The metaphase arrest of polar bodies depends on SAC pathway activation (Défachelles et al., 2015; Fischer et al., 2004; Pérez-Mongiovi et al., 2005). Therefore, we analyzed the localization of two well-conserved orthologs of the SAC pathway, BubR1 and Mad2 (Fig. 5). These proteins associate with unattached kinetochores and, in the case of BubR1, also to kinetochores lacking tension. Given that they inhibit the anaphase-promoting complex (APC/C), they are essential for maintaining metaphase arrest. BubR1 was present at polar body kinetochores in the wild-type (100%, *n*=23) and control BicD::GFP rescued eggs (93%, *n*=27) (Fig. 5Aa). However, in 43% of the *BicD*$^{hb\text{-}deGradFP}$ eggs, the meiotic products failed to recruit BubR1 to the kinetochores (*n*=35). The absence of BubR1 from the polar body kinetochores was observed in eggs in which polar bodies were fused into a single rosette (Fig. 5Ab) and in eggs showing many additional meiotic products (Fig. 5Ad,d′). The remaining *BicD*$^{hb\text{-}deGradFP}$ eggs showed either normal BubR1 recruitment (40%) or only a weak signal for kinetochore BubR1 (17%; Fig. 5Ac). Similar results were obtained for Mad2, whereby 69% of the *BicD*$^{hb\text{-}deGradFP}$ eggs analyzed did not show recruitment of Mad2 to the polar bodies (*n*=48; Fig. 5B). These data indicate that the failure to activate or maintain the metaphase arrest of polar bodies in the absence of BicD is probably the result of a failure to recruit the SAC components to the kinetochores or to maintain their association. That half of the polar bodies still recruited SAC components might also suggest that these nuclei are cycling in and out of metaphase arrest, duplicating their chromosomes. Altogether, these results suggest that, in *BicD*$^{hb\text{-}deGradFP}$ eggs, MII products do not arrest correctly in metaphase because of a failure to activate or maintain the SAC.

The BicD cargo and MT-stabilizing factor Chc localizes, similar to BicD, to centrosomes and mitotic and meiotic spindles

SAC function is disturb when spindle MT stability is perturbed. Given that BicD transports *Drosophila* Chc (Li et al., 2010; Vazquez-Pianzola et al., 2014) and vertebrate orthologs of this protein are needed to stabilize mitotic MTs (Fu et al., 2010; Royle et al., 2005), we analyzed Chc localization in *Drosophila* embryos.

Development (2022) 149, dev199944. doi:10.1242/dev.199944

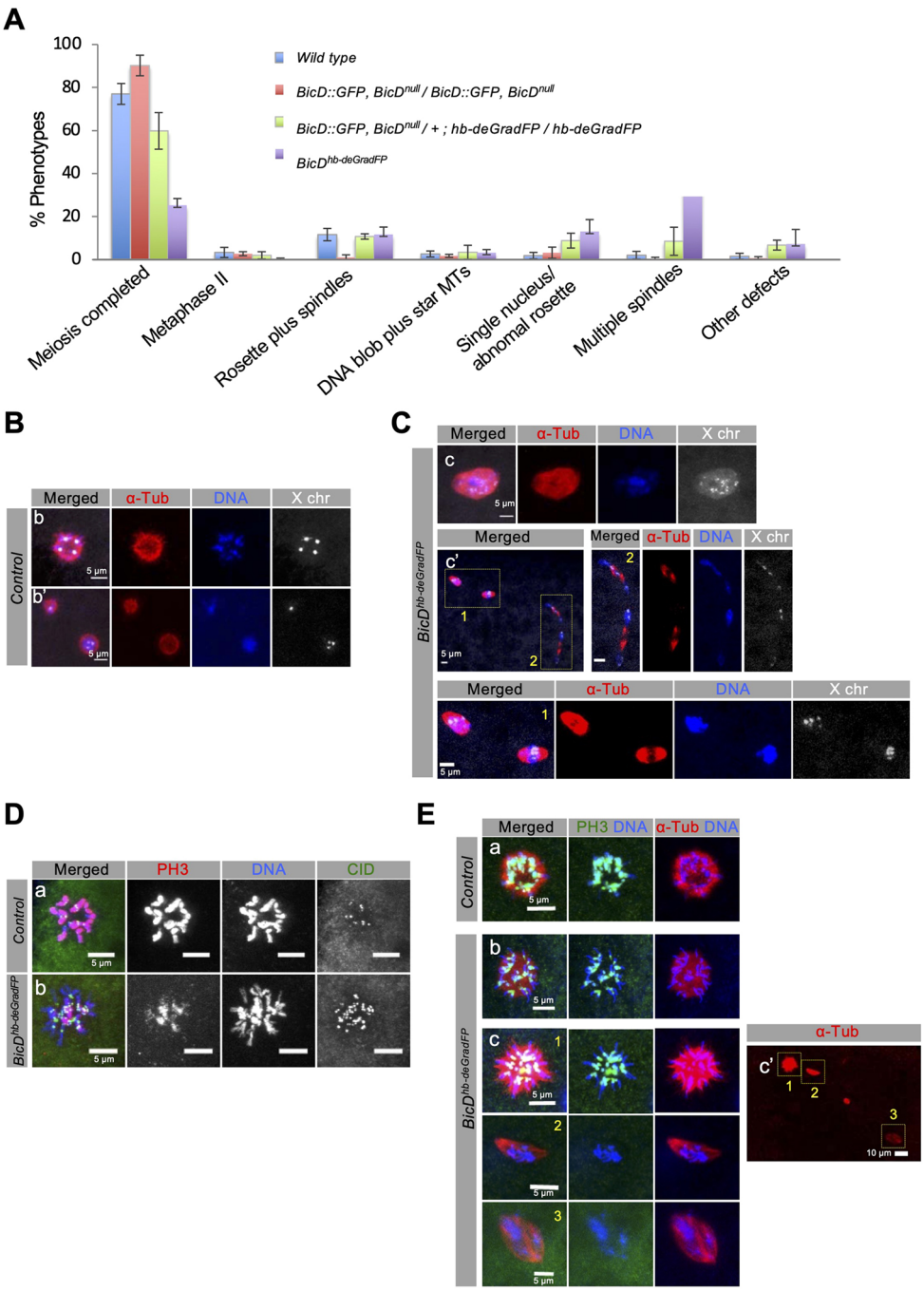

Fig. 4. Female meiotic products fail to arrest in metaphase and undergo extra rounds of replication in unfertilized *BicD*$^{hb\text{-}deGradFP}$ eggs. (A) 0-1 h-old unfertilized eggs from the indicated maternal genotypes stained for α-tubulin (red) and DNA (blue) and classified as follows: (1) eggs that apparently completed meiosis normally (up to four rosette-like structures that normally fuse into one single rosette); (2) eggs displaying a normal metaphase II tandem spindle; (3) eggs presenting one or two rosette-like structures plus one or two spindles (probably representing intermediate products of normal meiosis); (4) eggs with a big DNA blob surrounded by a star of MTs; (5) eggs containing a single nucleus/abnormal rosette; (6) eggs containing several spindles; (7) eggs with other defects. Data are means±s.d. of three or four independent egg collections (n1-n4). For wild type, n1=145, n2=95, n3=67; for *BicD::GFP, BicD*^{null}*/BicD::GFP*, n1=92, n2=72, n3=147; for *BicD*^{null}, *BicD::GFP/+; hb-deGradFP/hb-deGradFP*, n1=68, n2=46, n3=69, n4=67; and, for *BicD*$^{hb\text{-}deGradFP}$, n1=29, n2=45, n3=32 were scored. (B-C) Eggs from the same parental genotypes as in A subjected to FISH to detect the X chromosome (white) and stained for α-tubulin (red) and DNA (blue). (B) Meiotic products in control eggs (*BicD::GFP, BicD*^{null}) fused into a single (b) or two rosette-like structures (b′). (C) (c) *BicD*$^{hb\text{-}deGradFP}$ egg with a single abnormal rosette-like structure. (c′) *BicD*$^{hb\text{-}deGradFP}$ egg with more than four meiotic products. (D) Unfertilized wild-type and *BicD*$^{hb\text{-}deGradFP}$ eggs stained for CID (green, marking centromeres), PH3 (red) and DNA (blue). Of the single fused rosette nuclei in control eggs, 100% (12/12 confocal images) showed strong PH3 staining along the entire chromosomes. In 90.9% (10/11 confocal images) of these structures in *BicD*$^{hb\text{-}deGradFP}$ eggs, the signal was only enriched at the rosette central region. Of the single fused rosette-like nuclei in control eggs, 86% (6/7 confocal images) showed normal CID staining. In contrast, 63.7% (7/11) of these structures in *BicD*$^{hb\text{-}deGradFP}$ eggs showed an increased number of CID-positive dots. (E) Eggs were stained for α-tubulin (red), PH3 (green) and DNA (blue). (a) Meiotic products in control eggs fused into a single rosette. (b,c) *BicD*$^{hb\text{-}deGradFP}$ eggs either with a single abnormal rosette-like structure (b) or with more than four meiotic products (c). Images are *Z*-stack projections through the nuclei and yellow boxes mark the corresponding magnified nuclei.

Development (2022) 149, dev199944. doi:10.1242/dev.199944

However, antibodies available against Chc do not work well for immunostaining (Li et al., 2010); therefore, we analyzed the expression of Chc using tagged, yet functional, Chc fusions (Vazquez-Pianzola et al., 2014). Similar to BicD, Chc was enriched at the centrosomes and pericentrosomal regions during the entire cell cycle (Fig. 6A,B; Fig. S7A-C). During mitosis, Chc associated with the mitotic spindles (Fig. 6A-B; Fig. S7B,C). Moreover, also similar to BicD, Chc was enriched during cellularization near the plasma membrane between the nuclei, probably marking the sites where endocytic vesicles start to form (Fig. 6A; Fig. S7B) (Sokac and Wieschaus, 2008). *Drosophila* Clc showed a similar localization pattern during embryogenesis (Fig. S7D). Thus, Chc/Clc complex localization to the mitotic apparatus appears to be conserved between *Drosophila* and mammalian cells (Royle et al., 2005). Chc was not only present at the mitotic spindles, but also localized, similar to BicD, to the female meiotic II tandem spindles and the central aster (Fig. 6C).

Accurate localization of D-TACC, Msps and Clc at tandem meiotic spindles requires BicD

We focused on the early stages of meiosis II in eggs immediately released from MI arrest to pinpoint the first meiotic defects. Unfortunately, localization of tagged Chc was irreproducible because of the high cytoplasmic signal. Moreover, overexpressing a tagged Chc in the $BicD^{hb\text{-}deGradFP}$ background reduced the viability and fertility of the flies, preventing us from collecting enough embryos to analyze the meiotic spindles. Given that the Chc partner Clc is also present at the mitotic spindles together with Chc (Fig. S7D), we followed Clc localization during meiosis II (MII). Clc localized to the female MII tandem spindles and the central aster (Fig. 7A). We detected an unusual, strong accumulation of Clc at the central aster relative to the levels observed along the MII spindles in $BicD^{hb\text{-}deGradFP}$ tandem spindles compared with control spindles (Fig. 7A,A′). We then followed the localization of D-TACC and Msps because the spindle localization of their mammalian homologs is interdependent with that of Chc (Royle, 2012; Royle et al., 2005). In wild-type MII and anaphase II (AII) spindles, D-TACC and Msps were present on tandem spindles and enriched at the central aster (Fig. 7B,C). Additionally, D-TACC was weakly enriched at the spindle equator where the MT plus ends are located during metaphase II and AII (Fig. 7B, arrows). By contrast, Msps was enriched along both arms of the tandem spindles but stained the minus ends at the spindle poles more strongly (Fig. 7C, arrows). In $BicD^{hb\text{-}deGradFP}$ embryos, D-TACC and Msps localization along the tandem spindles was reduced compared with the control spindles (Fig. 7B,C). However, as in control spindles, D-TACC and Msps still showed enrichment at the central aster in $BicD^{hb\text{-}deGradFP}$ embryos (Fig. 7B,C). Accordingly, the signal intensity for D-TACC and Msps along the most superficial tandem spindle relative to the signal intensity observed in the central aster was significantly reduced in $BicD^{hb\text{-}deGradFP}$ MII spindles (Fig. 7B′,C′).

As a more direct approach to determining whether reduced BicD levels affect Chc localization, we analyzed the spindles of eggs laid by *BicD::GFP, BicD*^{null} females that expressed only one copy of the *hb-deGradFP* construct. In the background of this combination, which does not produce a phenotype on its own, we overexpressed Chc::mCherry. Eggs produced by such mothers did not develop and showed similar abnormal meiotic products to those observed in $BicD^{hb\text{-}deGRadFP}$ eggs (see below; Fig. 8D,F). In addition, we detected a mild reduction in the Chc::mCherry signal at the spindle compared with the signal in the central aster (Fig. S8A,A′). These results suggest that BicD is needed to localize clathrin, D-TACC and Msps accurately along the MII spindles.

The central aster is a disk-shaped structure that forms a non-centrosomal microtubule organizing center (ncMTOC) that produces astral MTs and contains several centrosomal proteins. To better understand how the MT polarity at the meiotic tandem spindle relates to the localization of the Clathrin/D-TACC/Msps complex, we stained eggs for minus- and plus-end MT markers. These stainings revealed that both plus- (Pav, Clip190 and EB1) and minus-end (Asp) MT markers were present at the central aster (Fig. S8B,C), suggesting that MTs with different orientations could also be present. Asp is also enriched at the ends of each meiotic spindle (Fig. S8B). The plus-end markers were distributed more evenly along the tandem spindle MTs compared with minus-end markers, and only Clip190 was slightly enriched near the DNA region (Fig. S8C). Given that TACC and Msps orthologs are MT plus-end-tracking proteins (Gutiérrez-Caballero et al., 2015; Lucaj et al., 2015; Nwagbara et al., 2014; Rutherford et al., 2016) and D-TACC is present at the centrosomes (Barros et al., 2005; Lee et al., 2001), this could explain why localization of clathrin, TACC and Msps is less affected in the central aster. It further suggests that BicD might be needed to stabilize or transport these proteins along the spindles. However, studying the dynamic movement of these proteins along the meiotic tandem spindle is challenging. Chc::mCherry signals, although present all along the spindles, showed a diffuse pattern, and we were unable to detect traceable particles along either the mitotic spindles or the arrested meiotic spindles in $BicD^{hb\text{-}deGradFP}$ and control eggs (Movies 5-7). However, we were able to detect Chc::mCherry particles or motile structures that moved along linear tracks resembling MTs during mitosis (Fig. S9A; Movies 8 and 9). Although only ‘escaper’ $BicD^{hb\text{-}deGradFP}$ eggs reached the mitotic division of the young embryo (because of the requirement for BicD for pronuclear migration and fusion), the net displacement and velocity of the Chc::mCherry particles detected in $BicD^{hb\text{-}deGradFP}$ embryos was reduced compared with the particles that we were able to track in control embryos (Fig. S9B-D′). The Chc particles we detected were rather large and resembled the Chc motile structures reported to move in a *BicD*-dependent manner in synaptic boutons and within the oocyte (Li et al., 2010; Vazquez-Pianzola et al., 2014). Smaller Chc-positive particles may also be subjected to transport along the spindles, but these were below the detection limit. These results suggest that BicD is required to move Chc-positive structures in linear tracks during mitosis.

Chc binds with the same domain to D-TACC and BicD, and D-TACC expression increases the BicD/Chc interaction

In mammals, Chc interacts directly with TACC3, and this interaction depends on the phosphorylation of Ser^{552} of TACC3 by Aurora A kinase (Fu et al., 2010; Lin et al., 2010). Given that D-TACC and clathrin fail to localize accurately on $BicD^{hb\text{-}deGradFP}$ MII spindles, we investigated, using a yeast two-hybrid (Y2H) assay and co-immunoprecipitation (IP) experiments, whether the *Drosophila* homologs of these proteins can interact with each other and with BicD (Fig. 8A,B). Indeed, full-length *Drosophila* Chc interacted with D-TACC in both assays.

The minimal region of mammalian isoform Chc22 that interacts with TACC3 spans amino acids 331-542 (Lin et al., 2010). Whereas the corresponding part of *Drosophila* $Chc^{329\text{-}542}$ did not interact with D-TACC in our assays (Fig. 8A), this region with a C-term extension ($Chc^{329\text{-}803}$) interacted with D-TACC almost as strongly as the full-length protein (Fig. 8A). Consistent with these results,

Development (2022) 149, dev199944. doi:10.1242/dev.199944

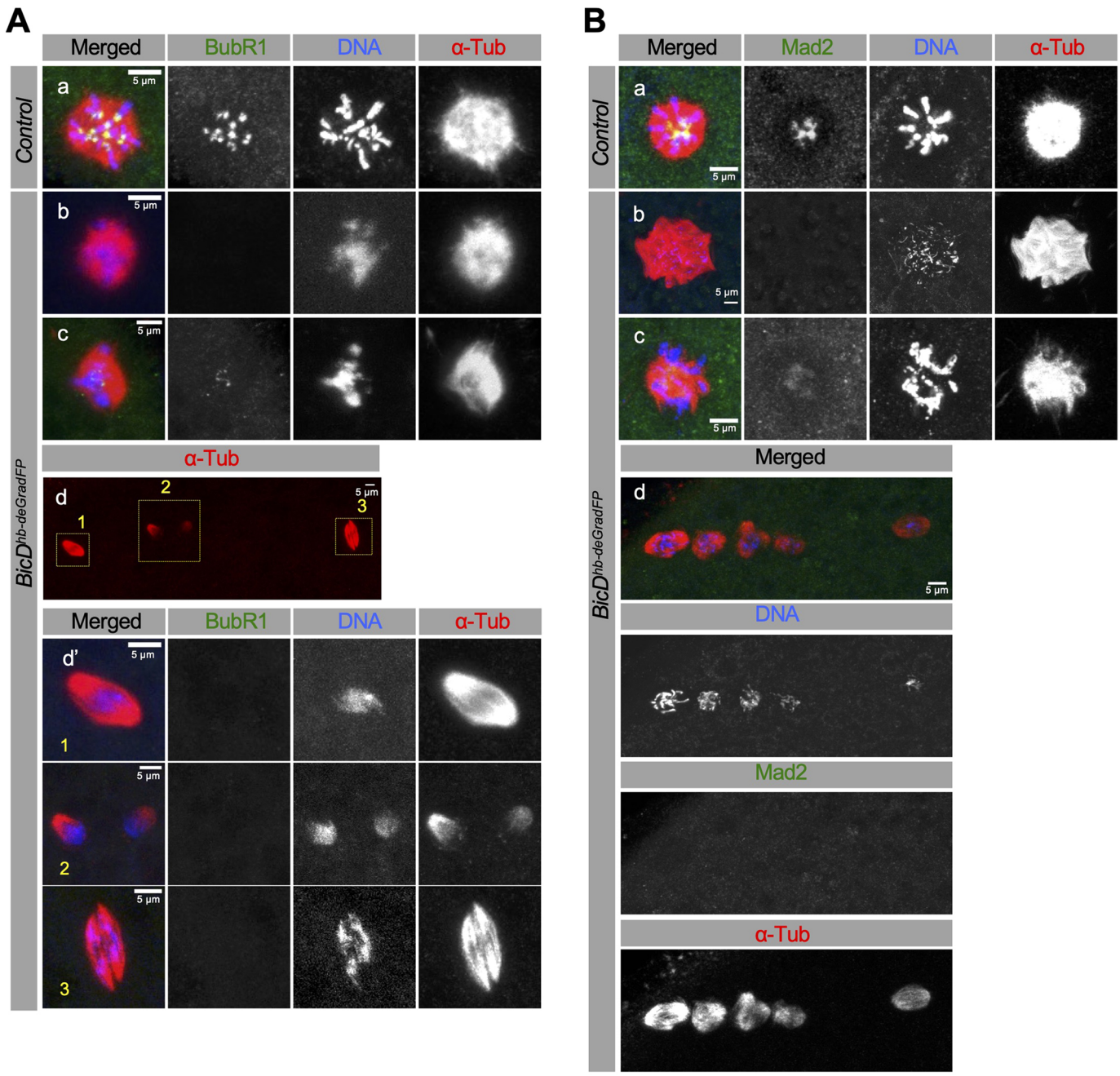

Fig. 5. BicD contributes to the recruitment of the SAC components BubR1 and Mad2 to the female meiotic products. (A-B) 0-1 h-old unfertilized eggs stained for α-tubulin (red), DNA (blue) and BubR1 (A) or Mad2 (B) (green). Control meiotic products [from either wild-type (Aa) or *BicD::GFP, BicD*^{null} (Ba) eggs] fused into a single rosette showed BubR1(Aa) and Mad2 (Ba) staining at the kinetochores. *BicD*$^{hb\text{-}deGradFP}$ egg containing a unique rosette-like polar body without BubR1 (Ab) or Mad2 (Bb) signals. *BicD*$^{hb\text{-}deGradFP}$ egg with only one polar body that stains only weakly for BubR1 (Ac) or Mad2 (Bc). *BicD*$^{hb\text{-}deGradFP}$ eggs in which the female meiotic products have replicated and do not stain for BubR1 (Ad,d′) or Mad2 (Bd). (Ad′) Magnified images of the indicated nuclei in Ad. Images are *Z*-stack projections through the nuclei.

Chc$^{329\text{-}542}$ was also unable to bind BicD (Fig. S10A). Chc$^{329\text{-}803}$ has been reported to contain the minimal BicD-binding region (Li et al., 2010). Consistently, Chc$^{329\text{-}803}$ interacted in our assays with the BicD C-terminal domain (CTD), a truncated version of BicD that interacts more strongly with its cargoes because it does not contain the BicD fold-back domain (Fig. S10B) (Li et al., 2010).

The Chc interaction with D-TACC was not abolished when the conserved Ser residue targeted by the Aurora A kinase was mutated to alanine (Ser^{863} in D-TACC, corresponds to Ser^{552} of the human protein; Fig. 8A; Fig. S10C). Nevertheless, the phosphomimetic substitution Ser^{863}>Asp in D-TACC increased its interaction with full-length Chc (Fig. S10C). These results suggest that phosphorylation of Ser^{863} may not be a prerequisite for the interaction of full-length D-TACC with Chc, at least in the Y2H system. However, it could enhance the interaction during mitosis and meiosis when the kinase is active.

The interaction of D-TACC with full-length Chc was observed under very stringent Y2H conditions (medium -L, -W, -H, -a;

Development (2022) 149, dev199944. doi:10.1242/dev.199944

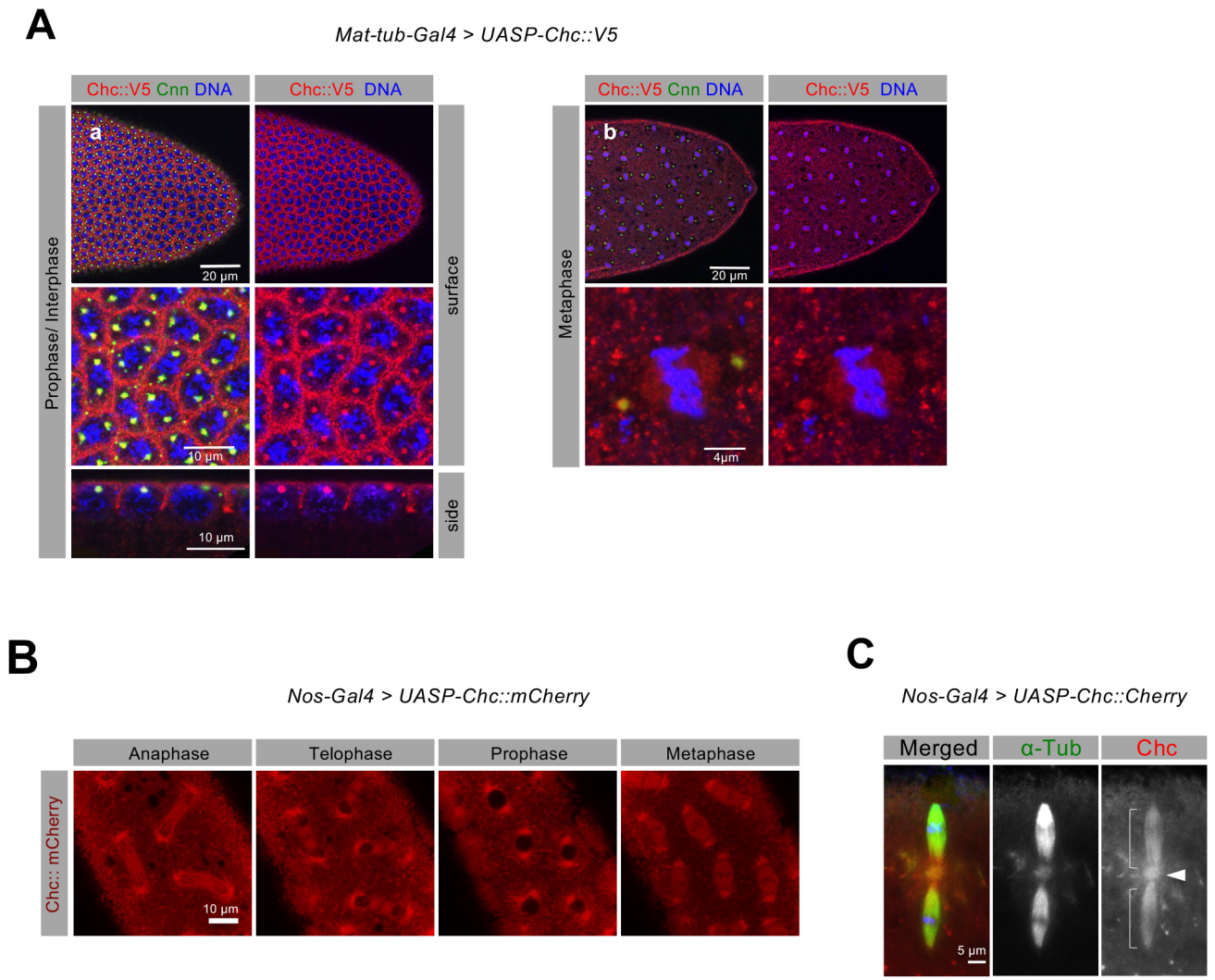

Fig. 6. Chc localizes to centrosomes and spindles during mitosis, and to MII spindles. (A) A Chc::V5-expressing cellular blastoderm (a) and a Chc::V5-expressing embryo in metaphase of nuclear cycle (NC)13 (b) stained for V5 (red) and Cnn (green). (B) Live imaging of Chc::mCherry-expressing embryos. (C) Chc::mCherry, detected with anti-mCherry antibodies (red), is present along both MII tandem spindles (brackets) and at the central aster (arrowhead).

Fig. S10C). In contrast, the interaction between Chc and BicD was only visible under less stringent conditions [medium -L, -W, -H +3 mM 3AT; Fig. S10A (Cagney et al., 2000)], suggesting that Chc interacts more strongly with D-TACC than with BicD in this system. Results from IP experiments using embryo extracts expressing a Myc::Chc fusion protein also supported this hypothesis. Myc::Chc was observed at low levels in BicD IPs. In contrast, the presence of BicD was not detected in the reverse IPs (with anti-Myc antibodies) as previously reported (Fig. 8B) (Vazquez-Pianzola et al., 2014). This result might be because of their weak interaction or the Myc tag interfering with the binding sites. Similarly, BicD antibodies also immunoprecipitated a Flag-tagged version of Chc (Fig. S11). In contrast, D-TACC strongly co-immunoprecipitated with Myc::Chc. However, no interaction was observed between D-TACC and BicD either by IP or in the Y2H system (Fig. 8B; Figs S10D and S11).

Given that we found that D-TACC and BicD bind to the same sequences in the Chc Ankle domain, Chc/BicD and Chc/D-TACC might only exist as mutually exclusive protein complexes. Thus, we tested whether the interaction between BicD-CTD and Chc can be outcompeted in yeast cells by coexpressing D-TACC (Fig. 8C). However, the opposite was the case. The interaction between BicD-CTD and Chc increased when D-TACC was also co-expressed in yeast cells (Fig. 8C). Given that Chc acts typically as a triskelion, higher-order complexes of the three Chc molecules could theoretically contain BicD or D-TACC, or both (see models in Fig. 8Cc′,c″). The presence of D-TACC might increase the formation or stability of this ternary complex, bringing additional molecules of BD/AD close together to upregulate the Gal4 promoter in the Y2H system.

High levels of Chc and D-TACC enhance the embryonic arrest phenotype of *BicD$^{hb\text{-}deGradFP}$* embryos

BicD::GFP, BicD^{null} females, expressing only one copy of the *hb-deGradFP* construct (*BicD::GFP, BicD^{null}*; *hb-deGradFP-bcd 3′ UTR/+*) produced embryos that showed a reduction in BicD::GFP levels of only 30% on western blot (Fig. S2B,C), mainly developed normally and hatched into larvae (Figs 2D,E and 8D). However, when these females expressed an additional copy of a *Chc* or D-TACC transgene, 80-95% of their progeny failed to hatch as larvae. Instead, they arrested with the same abnormal nuclei phenotype observed in *BicD$^{hb\text{-}deGRadFP}$* embryos (Fig. 8D-G; Fig. S12). Overexpressing Chc or D-TACC alone in females expressing a wild-

Development (2022) 149, dev199944. doi:10.1242/dev.199944

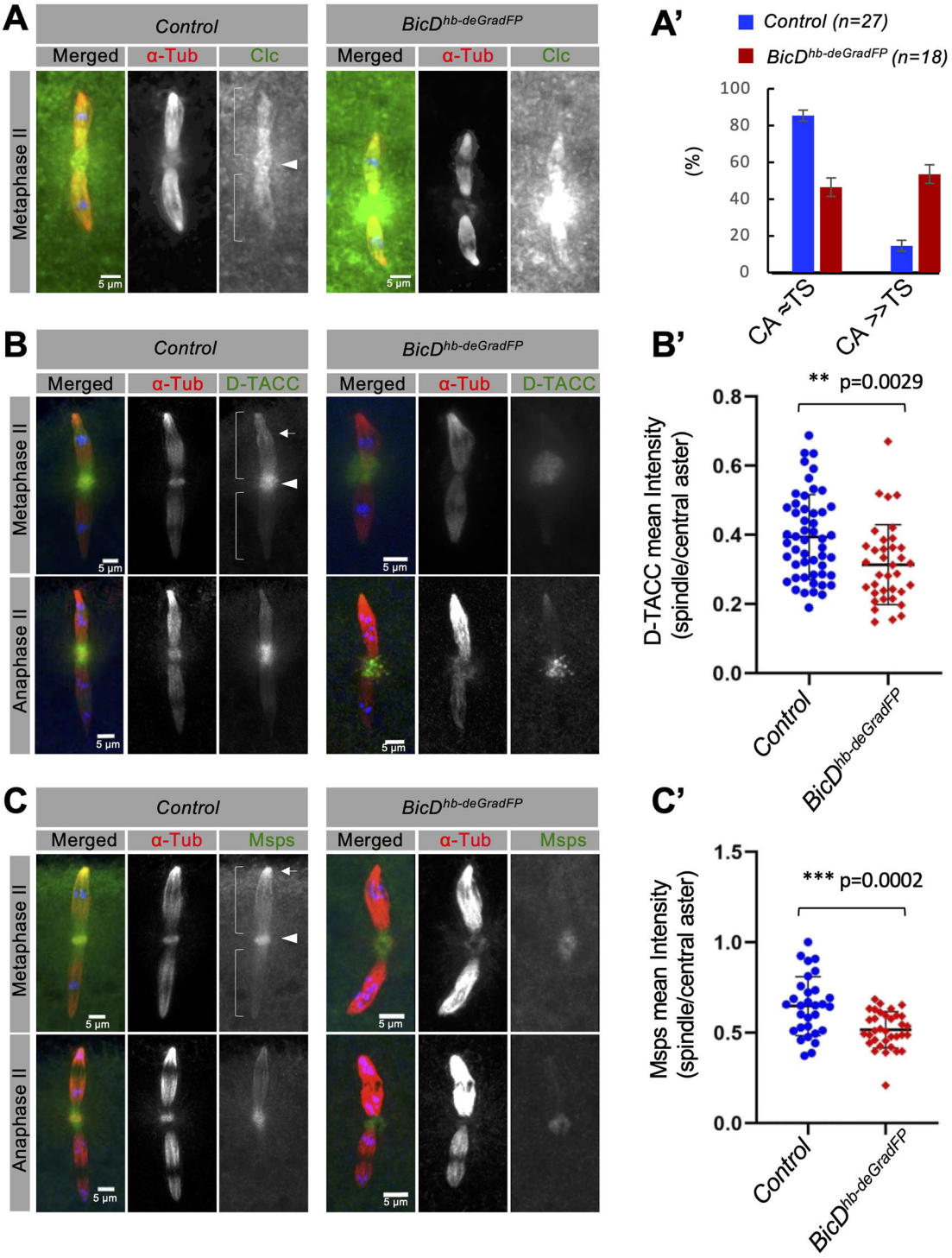

Fig. 7. Accurate localization of D-TACC, Msps and clathrin at MII tandem spindles requires BicD. Controls [laid by wild-type flies (A) or homozygous *BicD::GFP, BicD*^{null} (B-C)] and *BicD*$^{hb\text{-}deGradFP}$ embryos stained for α-tubulin (red) and either Clc (A), D-TACC (B) or Msps (C) (green). DNA is stained blue. The tandem spindles (brackets), spindle minus (arrow in C) and plus-ends (arrow in B) and the central aster (arrowheads) are indicated. (A) Maximum intensity projection images subjected to depth correction (see Materials and Methods). Clc hyperaccumulates at the central aster in *BicD*$^{hb\text{-}deGradFP}$ eggs. (A′) Percentage of embryos showing similar signal intensity along the tandem spindles (TS) and the central aster (CA) (CA≈TS), and embryos with hyperaccumulation of Clc at the central aster (CA>>TS) is shown for both genotypes. *n*=sum of embryos scored for each genotype: Control, n1=16, n2=18; *BicD*$^{hb\text{-}deGradFP}$, n1=14, n2=10; two experiments. Two independent researchers performed the qualitative scoring blindly. Data are means±s.d. (B-C) Maximum intensity projection images are shown. The signal on the most superficial spindle (top of image) is often stronger than the signal from the inner spindle because of the depth of the sample and antibody penetration issues. The signal in the inner spindle is also often masked by the cytoplasmic signal above. Compared with the signal intensity in the central aster, D-TACC and Msps signals on the *BicD*$^{hb\text{-}deGradFP}$ spindles are reduced. (B′,C′) Mean fluorescent signal intensity ratio (signal in the most superficial spindle vs signal in central aster) for D-TACC (B′) and Msps (C′) was quantified for each imaged MII and AII spindle. (B′) Control, *n*=51; *BicD*$^{hb\text{-}deGradFP}$, *n*=36; three experiments. (C′) Control, *n*=30; *BicD*$^{hb\text{-}deGradFP}$, *n*=34; two experiments. Data are means±s.d., analyzed by unpaired Student's *t*-test: ***P*<0.01; ****P*<0.001.

Development (2022) 149, dev199944. doi:10.1242/dev.199944

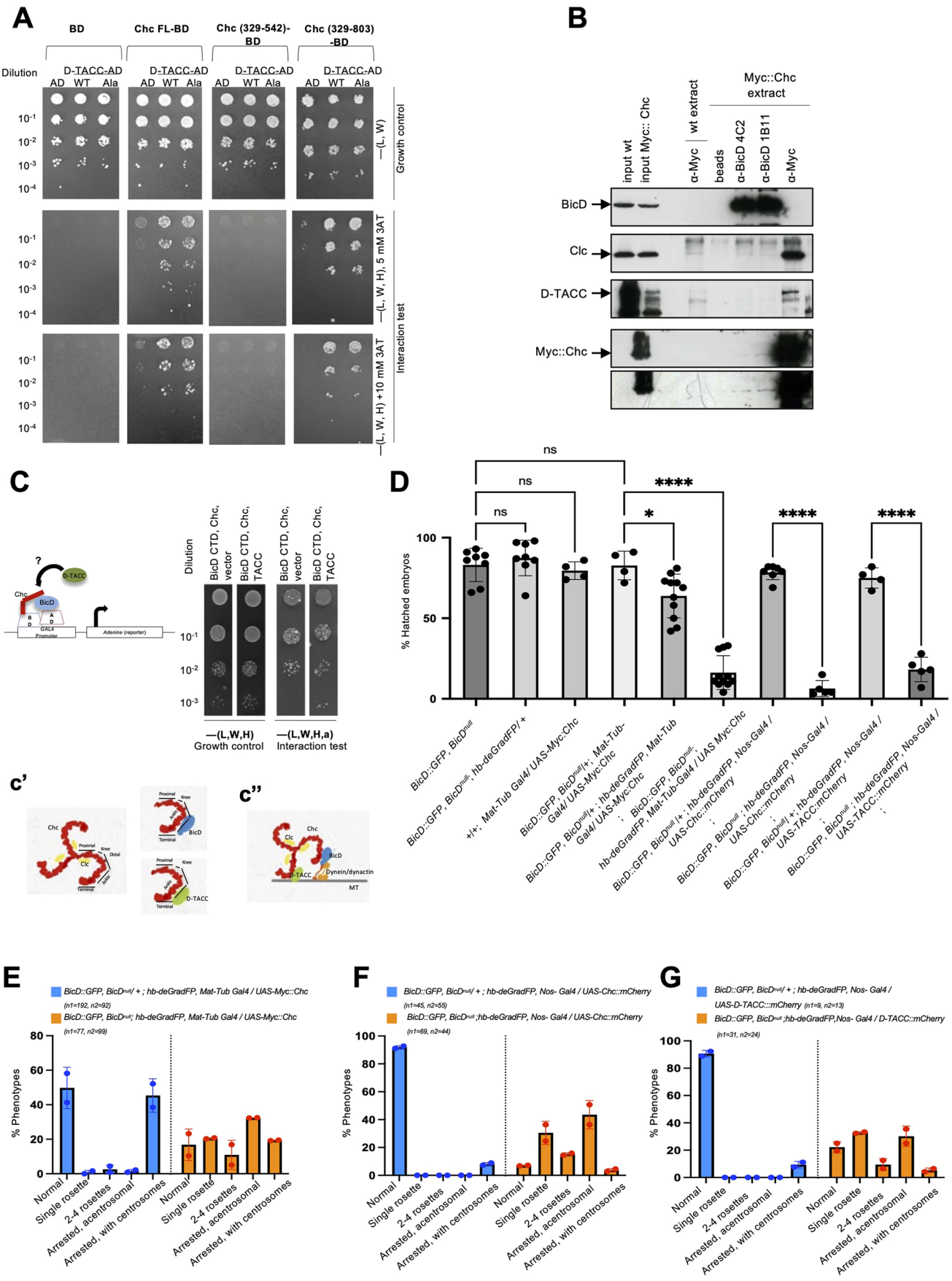

Fig. 8. See next page for legend.

Development (2022) 149, dev199944. doi:10.1242/dev.199944

Fig. 8. *Drosophila* Chc binds to D-TACC through the same domain it uses to interact with BicD, and *BicD* and *Chc* genetically interact in embryos. (A) Y2H interaction tests. Full-length (FL) and partial Chc fragments ($Chc^{329-542}$ and $Chc^{329-803}$), respectively, were fused to the DNA BD. Full-length D-TACC wild type (WT) and $D\text{-}TACC^{S863A}$ were fused to the AD. Empty vectors served as negative controls. (B) IP of total embryo extracts expressing a Myc-tagged Chc fusion protein (Myc::Chc). Antibodies used for IP are indicated on top. Beads alone and anti-Myc pulldowns in wild-type (wt) embryo extracts were used as negative controls. Western blots of the IP material tested for the presence of BicD, Clc, D-TACC and Myc::Chc. Input represents 0.15% of the cytoplasmic extract used for each IP. Bottom panel shows a longer exposure of the Myc::Chc blot. (C) Interaction between BicD CTD-AD and full-length Chc fused to the BD was tested in the presence of either an empty vector or a vector expressing D-TACC. The co-expression of TACC increases the BicD-CTD/Chc interaction. (c′) Models depicting the interactions between Chc, Clc, BicD and D-TACC. Chc is known to form trimers with Clc (triskelion). BicD and D-TACC both bind to the Ankle region of Chc. (c″) Model of the formation of putative ternary complexes on the MT. (D) Percentage of embryos that hatched into larvae (their maternal genotypes are indicated). An increase in the number of embryos arrested in embryogenesis was observed even in embryos expressing a wt copy of *BicD* when Chc was expressed under the strong maternal tubulin promoter. Between 50 and 200 eggs were counted for each replicate. (E-G) 30-60 min-old embryos with the indicated maternal genotypes stained for α-tubulin (red), Cnn (green) and DNA (blue). Percentage of embryos displaying the different phenotypes. Although the ratio of the number of eggs arrested with centrosomes compared with those without vary in the different genotypes (because overexpression of Chc and D-TACC increased the frequency of unfertilized eggs), the eggs show a early arrest phenotype similar to that observed in $BicD^{hb\text{-}deGradFP}$. Two independent collections were analyzed. Error bars show the s.d. Data in D analyzed with a one-way ANOVA; *P<0.05; ****P<0.0001.

type copy of *BicD* did not produce visible phenotypes in their embryos, suggesting that high levels of either Chc or D-TACC in a BicD-reduced background are responsible for the phenotypes. Moreover, these embryos showed the same early arrest phenotypes observed in $BicD^{hb\text{-}deGradFP}$ embryos (Fig. 8E-G; Fig. S12).

Similar to BicD, D-TACC is required for pronuclear fusion and cell cycle arrest of the male pronucleus and female meiotic products

$d\text{-}tacc^{1}$ ($tacc^{1}$) mutant mothers lay eggs with reduced D-TACC protein levels, and most of these embryos fail to develop (Gergely et al., 2000). Of the male progeny laid by $d\text{-}tacc^{1}/Df(3R)110$ females, only 25.8% showed signals for the X and Y chromosomes in each zygotic nucleus, indicating that they had undergone pronuclear fusion (Fig. S13A). Most of the male progeny (74.2%) had at least one internal nucleus marked for the Y chromosome and no X-chromosomal signal (Fig. S13B-D), showing that, in $d\text{-}tacc^{1}$ embryos, pronuclear fusion is strongly compromised. Of those embryos that did not perform pronuclear fusion, 30.4% showed normal cell cycle arrest of the female and male meiotic products (Fig. S13B). In 47.85% of those embryos (Fig. S13C), the paternal pronucleus underwent additional divisions with no over-replication of the female meiotic products. Only 21.7% of them showed replication of the female meiotic and male-derived nuclei (Fig. S13D). The lower penetrance of this female meiosis phenotype compared with that observed in $BicD^{hb\text{-}deGRadFP}$ eggs (70% of the arrested eggs) could be because $d\text{-}tacc^{1}$ embryos produce sufficient levels of D-TACC to rescue the female meiosis phenotype (Gergely et al., 2000). Therefore, BicD and D-TACC are required for pronuclear fusion and metaphase arrest of the male pronucleus and the female meiotic products. We also observed abnormal meiosis with delayed polar body extrusion in eggs from *C. elegans* fed with bacteria expressing double-strand (ds)RNA against *tac-1* (Fig. 9). Moreover, pointing to a conserved role for these proteins in pronuclear fusion, we also found that eggs from worms fed with dsRNA against *bicd-1*, *chc-1* and *tac-1* did not undergo pronuclear fusion (Fig. 9).

DISCUSSION

A useful strategy to study the effect of lethal or female sterile mutations in early embryogenesis reveals that *BicD* is required for meiosis II and pronuclear fusion

We found that BicD localizes to the female tandem spindles and the central aster during MII. After fertilization, BicD also localizes to the mitotic spindles and the centrosomes. $BicD^{null}$ mutants rarely survive and are sterile, but we generated embryos with reduced levels of BicD at the beginning of embryogenesis ($BicD^{hb\text{-}deGradFP}$ embryos) by setting up a strategy based on the deGradFP technique. Consistent with BicD localization at the female MII spindles, we discovered that $BicD^{hb\text{-}deGradFP}$ embryos arrest development, displaying aberrant meiotic products and no pronuclear fusion. Especially if combined with the CRIPSP-Cas9 strategy first to produce functional GFP-tagged proteins of interest, the construct designed in this study could be helpful for studying the role of female-sterile and lethal mutations during very early embryonic development (Nag et al., 2018).

Connecting BicD to the SAC pathway

In unfertilized $BicD^{hb\text{-}deGradFP}$ eggs, the female meiotic products were not arrested in metaphase as normally happens. Instead, they underwent additional rounds of replication. They failed to recruit or maintain the recruitment of the SAC pathway components BubR1 and Mad2, which are normally present at the kinetochores in the wild-type female meiotic polar bodies. Interestingly, in *Drosophila* eggs mutated for *Rod*, *mps1* and *BubR1*, well-conserved orthologs of the SAC pathway, the polar bodies also cannot remain in a SAC-dependent metaphase-like state and decondense their chromatin (Défachelles et al., 2015; Fischer et al., 2004; Pérez-Mongiovi et al., 2005). Furthermore, in these mutants, the polar bodies cycle in and out of M-phase, replicating their chromosomes similarly to those in $BicD^{hb\text{-}deGradFP}$ eggs. Thus, it appears that BicD functions to localize the SAC components to induce and/or maintain metaphase arrest of the polar bodies. Several mechanisms could explain the failure to maintain SAC activation observed in $BicD^{hb\text{-}deGradFP}$ embryos. BicD might be needed to recruit the SAC components to kinetochores directly. By contrast, during mitosis, the Rod-Zw10-Zwilch (RZZ) complex binds to the outer kinetochore region and recruits Mad2, Spindly and the dynactin complex. Spindly and dynactin act cooperatively to recruit dynein, which then transports the SAC components along the MTs away from kinetochores as a mechanism to trigger checkpoint silencing and anaphase onset (Basto et al., 2004; Howell et al., 2001; Wojcik et al., 2001; Griffis et al., 2007). Given that the BicD N-terminal domain binds dynein and dynactin and promotes their interaction (Splinter et al., 2012), it is also possible that BicD helps to move the SAC components away from the kinetochores. If this does not happen, the SAC remains persistently activated. We also found that BicD activity in $BicD^{hb\text{-}deGradFP}$ embryos is insufficient to localize clathrin, TACC and Msps efficiently along the MTs of the spindle. During mitosis, impairment of MT motors, such as dynein, and treatments that prevent the TACC/clathrin complex from binding to the mitotic spindles and affecting K-fiber stability, also persistently activate the SAC (Rieder and Maiato, 2004; Royle et al., 2005). Thus, reduced levels of BicD in $BicD^{hb\text{-}deGradFP}$ embryos could additionally trigger SAC hyperactivation through its role in stabilizing the K-fibers. Although our data strongly suggest that the lack of BicD

Development (2022) 149, dev199944. doi:10.1242/dev.199944

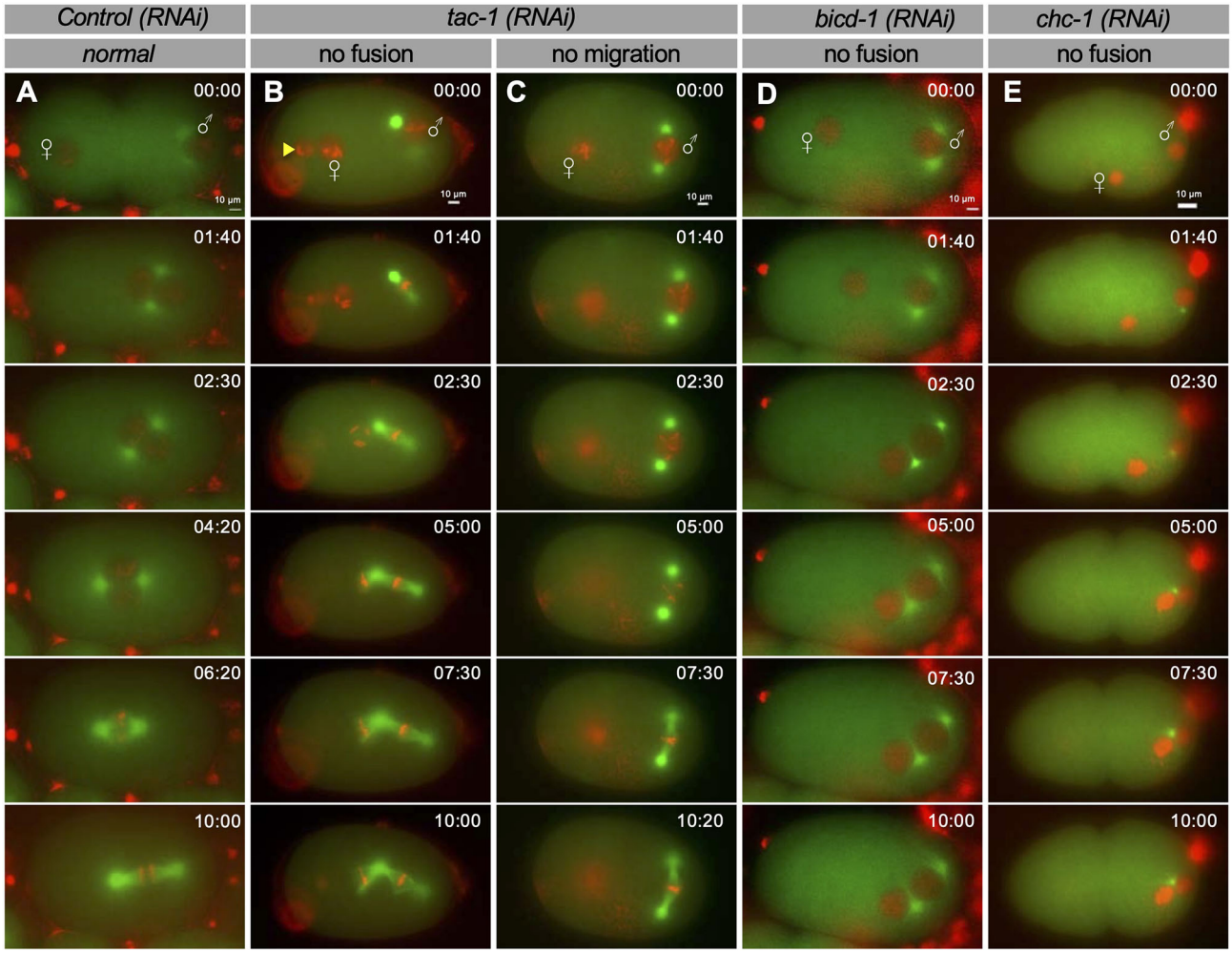

Fig. 9. *Caenorhabditis elegans chc-1*, *bicd-1* and *tac-1* are required for pronuclear fusion. Time-lapse images of embryos expressing *H2B::mCherry* and *α-tubulin::GFP*. Female and male pronuclei and the elapsed time (in minutes and seconds) from the start of the movie are indicated. (A) Control embryos grown on either regular food (6/6) or control empty vector RNAi food (14/15) progressed normally from meiosis to the formation of the first mitotic spindle. The female pronucleus at the embryo anterior (left) and the male pronucleus and its two associated centrioles at the posterior (right) are indicated. The female pronucleus moved towards the posterior pole and the male pronucleus and both met at the posterior. After centration and rotation, the pronuclei fused to form the first mitotic spindle at the center of the zygote along the anteroposterior (A-P) axis. (B-C) *tac-1(RNAi)* embryos showed meiosis and pronuclear fusion defects as previously described using differential interference contrast (DIC) microscopy (Bellanger et al., 2007). (B) *tac-1(RNAi)* embryo showing abnormal meiosis with delayed polar body extrusion (arrowhead) and no pronuclear fusion (2/5 analyzed). The male pronucleus formed a spindle on its own at the posterior pole, and both pronuclei met at the posterior pole, forming a common spindle without pronuclear fusion. (C) *tac-1(RNAi)* embryo with normal meiosis but defective female pronuclear migration and no pronuclear fusion (2/5 embryos). The male pronucleus formed a spindle at the posterior pole. (D) Delayed female pronuclear migration was observed in a fraction of the *bicd-1(RNAi)* embryos (3/10). Although both pronuclei ultimately met at the posterior, they neither fused nor moved towards the center of the embryo. (E) Animals fed with *chc-1* dsRNA food looked sick and carried few progenies in the uterus. The few living *chc-1(RNAi)* embryos showed delayed female pronuclear migration, no pronuclear fusion and lack of centration (2/4 embryos). Additional phenotypes observed are described in Fig. S14.

contributes to SAC defects through its role in localizing clathrin, D-TACC and Msps, further work is needed to elucidate whether BicD also acts more directly by binding to, and localizing, the SAC components, or indirectly by affecting the function of dynein.

Whereas persistent SAC activation leads to metaphase arrest and delayed meiosis (D-meiosis), this delay is known to be rarely permanent, at least during mitosis. Most cells that cannot satisfy the SAC ultimately escape delayed mitosis (D-mitosis) and enter G1 as tetraploid cells by a currently poorly understood mechanism (Rieder and Maiato, 2004). It is possible that, in $BicD^{hb\text{-}deGradFP}$, the SAC pathway is constantly activated, delaying meiosis. However, at one point, the nuclei might escape metaphase II arrest, cycling in and out of M-phase, thereby replicating their chromosomes and decondensing their chromatin. The fact that female meiotic products over-replicate in $BicD^{hb\text{-}deGradFP}$ eggs and show no or only pericentromeric PH3 staining supports the notion that these nuclei are on an in-out metaphase arrest phase. That meiotic products in about half of the $BicD^{hb\text{-}deGradFP}$ embryos failed to stain for the SAC components BubR1 and Mad2 supports this hypothesis.

Connecting BicD to the D-TACC/Msps/clathrin complex

Chc, its partner Clc and BicD are enriched at mitotic spindles and centrosomes. Furthermore, these proteins and the clathrin-interacting partners D-TACC and Msps localize to the tandem spindles and the central aster of the female MII apparatus. The interaction of *Drosophila* Chc with D-TACC is conserved, and Chc interacts through the same protein domain directly with D-TACC and BicD (Fu et al., 2010; Lin et al., 2010). Moreover, BicD is needed for localizing D-TACC, Msps and clathrin throughout the

Development (2022) 149, dev199944. doi:10.1242/dev.199944

MII tandem spindles. The TACC3/Chc interaction was proposed to form a domain in tandem to bind spindle MTs (Hood et al., 2013). We hypothesize that BicD could help recruit Chc to the MTs by association with dynein. Given that Chc usually acts as a trimer with Clc (triskelion), each Chc might interact with either BicD or D-TACC. Thus, a mixed complex could be formed, and BicD might help to move, recruit or stabilize Chc and D-TACC along the spindles via the interaction of BicD/Chc in the same trimer (model in Fig. 8Cc″). The fact that expression of D-TACC enhances the Chc/BicD interaction and that overexpression of *Chc* and *D-TACC* (*tacc*) arrested early development in a background in which BicD is reduced to a level that does not produce visible phenotypes on its own, supports this model. Our results suggest that, with respect to BicD, the levels of D-TACC and Chc should be tightly balanced for these proteins to perform their normal function during early development, as has been shown previously for other BicD transport processes (Vazquez-Pianzola et al., 2014).

Role of BicD in pronuclear fusion

BicD has a role in pronuclear fusion that is conserved during evolution given that *C. elegans* eggs depleted for *bicd-1* also failed to undergo pronuclear fusion. Moreover, *Drosophila D-TACC* and *C. elegans chc-1* and *tac-1* are also needed for pronuclear fusion. These genes might be required indirectly through their role in meiosis because preliminary data suggest that MII is also compromised in *bicd-1* and *chc-1* dsRNA-fed worms (Fig. S14). Alternatively, they might play a more direct role in pronuclear migration, which depends on dynein and MTs in bovine, primate and *C. elegans* embryos (Gönczy et al., 1999; Payne et al., 2003). This would then suggest that the underlying mechanism may be used to build correctly or stabilize different types of MT. Determining their precise mechanistic involvement in pronuclear fusion is an interesting question for further studies.

MATERIALS AND METHODS

Drosophila stocks

P{matα4-GAL-VP16}, *Nos-Gal4:Vp16*, *UAS-Clc::GFP*, *Histone::RFP*, C(1;Y)1, y1w: y+/0 and *C(1)RM, y1 v1/0* stocks were obtained from the Bloomington *Drosophila* Stock Center (NIH P400D018537). Flies containing the genome rescue transgenes p*CHC3+* (Bazinet et al., 1993) and *4C-CHC* (Kasprowicz et al., 2008) were kindly provided by C. Bazinet (St John's University, Jamaica, NY, USA) and P. Verstreken (VIB-KU Leuven Center for Brain and Disease Research, and Leuven Brain Institute, Leuven, Belgium), respectively. *D-tacc*^{1} and *Df 3R(110)*, covering the *tacc* locus, were provided by J. Raff (University of Oxford, UK) (Gergely et al., 2000). S. Bullock (MRC Laboratory of Molecular Biology, Cambridge, UK) provided the *UAS-Chc::eGFP* and *UAS-Chc::mCherry* flies (Li et al., 2010). Transgenic *pUASP-Chc-V5-K10-AttB* and *pUASP-myc-chc-K10-AttB* flies were described previously (Vazquez-Pianzola et al., 2014). *Df(2L)Exel7068* (Exelixis) were used as *BicD*-deficient flies (*BicDDf*). The *BicD*^{null} allele, *BicDr5*, the *BicD::GFP* flies and the method to generate *BicD*^{mom} females were described previously (Paré and Suter, 2000; Ran et al., 1994; Swan and Suter, 1996; Vazquez-Pianzola et al., 2014). *white* (*w*) flies were used as controls.

To produce unfertilized eggs, virgin *w* females were crossed to *C(1;Y)1, y1w: y+/0* males to generate XO males that are phenotypically normal but sterile. XO males were then crossed to virgin females of the desired phenotype. Eggs laid by these females were not fertilized.

DNA constructs and generation of transgenic flies

The generation of the flies expressing the *hb-deGRadFP* construct was as follows. First, we cloned the NSlmb-VhhGFP4 sequence [which comprises the F-box domain contained in the N-terminal region of the *Drosophila* supernumerary limbs (Slmb) protein fused to the GFP-binding nanobody VhhGFP4 sequence] described by Caussinus and colleagues (2011). Then, NSlmb-VhhGFP4 was cloned under the *hb* minimal maternal promoter containing the 5′-UTR leader of the maternal 3.2 Kb *hb* transcript and combined with the *bcd* 3′-UTR, following the strategy used by Schulz and Tautz, who used it to induce an artificial Hb gradient in embryos (Schulz and Tautz, 1995). The *Nslmb-VhhGFP4* sequence was PCR amplified with specific primers bearing BamHI and KpnI sites using the plasmid pUAS-Nslmb-VhhGFP4 as the template (Caussinus et al., 2011).

Primer sequences were as follows: Nano-GFP-sense-BamHI (GGA-TCCATGATGAAAATGGAGACTGACAAAAT); Nano-GFP-anti-Kpn (GGTACCTTAGCTGGAGACGGTGACCTGGGTG). PCR products were subcloned into the same sites of the pCaSper-AttB vector to create the plasmid pCasper-AttB-Nslmb-VhhGFP4 (or pw+GFP nanobody). A 1.5 kbp fragment of the *bicoid* 3′-UTR genomic region (Berleth et al., 1988) was amplified from a genomic library using specific primers containing KpnI and NotI restrictions sites: bcd 3′-UTR sense-Kpn I (GGTAC-CACGCGTAGAAAGTTAGGTCTAGTCC); bcd 3′-UTR anti-Not I (GCGGCCGCGCTAGTGCTGCCTGTACAGTGTCT). The insert was cloned by T-end ligation into the pCR2.1 TOPO vector and later subcloned into the KpnI/NotI sites of pCasper-AttB-Nslmb-VhhGFP4 to generate the pCasper-AttB-Nslmb-VhhGFP4-bcd 3′-UTR construct (or pw+GFP nano-body-bcd 3′-UTR). The minimal maternal *hb* promoter region together with the 5′-UTR leader of the maternal 3.2 kb *hb* transcript were amplified using as a template the Lac8.0 construct already described (Margolis et al., 1994) and kindly provided by J. Posakony (University of California San Diego, La Jolla, USA). Primers for this amplification contained flanking BglII and BamHI sites and were as follows: Hb-pr-sense–BglII (AG-ATCTTCCGGATCAGCGGCGCTGATCCTGC); Hb-pr–Anti-BamHI (GGATCCCTTGGCGGCTCTAGACGGCTTGCGGACAGTCCAAGTG-CAATTC). Inserts were further cloned into the BamHI of Nslmb-VhhGFP4-bcd 3′-UTR to generate Hb-Nslmb-VhhGFP4-bcd 3′-UTR (or pw+Hb-GFP nanobody-bcd 3′-UTR). This final plasmid was injected into embryos containing the ZH-attP-14/3R-86F landing platform to generate flies expressing the *hb-deGradFP* construct.

The *don Juan (Dj)::mCherry* construct to produce transgenic flies was generated as follows. First, the mCherry region was PCR amplified with primers containing BamHI and HindIII sites using pC4-SqhP-mCherry plasmid as the template [a gift from R. Levayer (Institut Pasteur, Paris, France)]. The reverse primer added a GS-rich region as a linker and removed the stop codon. The primers were as follows: mCherry fw, GAA TAT GGA TCC GGT TCA GGT GTG AGC AAG GGC GAG GAG G; mCherry rev, GAC GAT AAG CTT TTA CTT GTA CAG CTC GTC CAT GCC. Then, the amplified fragment was further subcloned into the BamHI/HindIII sites of the plasmid *pw+SnattB* (Koch et al., 2009) to generate the plasmid *pw+attB*-mCherry. Next, the genomic region containing the minimal promoter, the 5′-UTR, and the open reading frame (ORF) of *Dj* was PCR amplified from genomic fly DNA using primers containing EcoRI and BamHI sites and cloned into the same sites of *pw+attB*-mCherry to generate the final construct, *pw+attB-Dj::mCherry*. The primers were as follows: dj promoter fw, GAC GAT GAA TTC ATG GAC GGA AGG ACA TTT TCA G; dj promoter rev, GACGAT GGA TCC CTT TTT CTT GCA TTT GTC TTT TTT AGC C. Finally, this construct was further injected into flies containing the ZH-attP-52/3L-64A landing platform for transgenesis.

Hatching rate determination and embryo development

Hatching rates were scored as follows. First, virgin females of the desired genotype were crossed to control *w* males. Females were allowed to lay eggs on agar plates for several hours or overnight. Around 100-200 embryos were marked in the plate and further developed for 48 h at 25°C. After 48 h, embryos that did not hatch were counted. Then, 30-60 min or 2-5 h-old embryos were collected for scoring embryo development. Embryos were then fixed and stained to detect both α-tubulin and DNA to score the development stage.

Western blot

The preparation of ovaries for western blots was as follows. Seven pairs of ovaries were collected from well fed 2- to 3-day-old *Drosophila* female flies in 20 µl of SDS-sample buffer, boiled for 2 min, vortexed for 15 s, and

Development (2022) 149, dev199944. doi:10.1242/dev.199944

boiled for another 8 min, before being loaded onto an SDS-PAGE gel. Approximately 15-20 µl of embryos of the desire stage were collected, dechorionated and resuspended in 30-50 µl of SDS-sample buffer. After homogenization in an eppendorf tube with a plastic pestle, they were boiled for 3 min, centrifuged at 16,000 ***g*** for 1 min and then different amounts (2-10 µl) were loaded onto the SDS-PAGE gel. Western blots were performed using mouse monoclonal anti-BicD antibodies [1:10 dilution mixture of 1B11 and 4C2, cell culture supernatant produced in our laboratory (Suter and Steward, 1991)], mouse anti-α-tubulin [1:2000 cell culture supernatant, Developmental Studies Hybridoma Bank (DSHB), clone AA4.3], rabbit anti-mammalian Chc [1:500, a gift from M. S. Robinson (University of Cambridge, Addenbrooke's Hospital, Cambridge, UK) (Hirst et al., 2009)], rabbit anti-GFP (1:3000, ImmunoKontact, 210-PS-1GFP), rabbit anti-Clc [1:3000, a gift from D. Graeme (University of Southern California, Los Angeles, USA) (Heerssen et al., 2008)], mouse monoclonal anti-Myc 9E10 [1:5 cell culture supernatant, DSHB, clone 9E 10), rabbit anti-D-TACC UT316 [1:10,000, a gift from T. Megraw (Florida State University, Tallahassee, USA) (Kao and Megraw, 2009)], anti-TACC [1:500, a gift from J. Raff (Sir William Dunn School of Pathology, University of Oxford, UK)] and rabbit anti-Flag (1:320, Sigma, F7423). Primary antibodies were detected using horseradish peroxidase (HRP)-conjugated secondary antibodies [1:10,000; GE Healthcare, NA934V, LNA931V/AH). To detect deGRadFP expressed from the *hb-deGRadFP* construct, anti-llama IgG-heavy and light chain antibodies (1:500, Bethyl, A160-100A) were used and developed using anti-goat IgG (H+L)-HRP conjugated antibodies (1:500, Invitrogen, A15999). We found that, although the *hb-deGRadFP* construct expressed a fusion protein between the Fbox and the Vhh (and not the whole immunoglobulin) of a llama nanobody that recognized GFP, Vhh was still recognized by the commercially available anti-llama serum made in rabbits from Bethyl. Indeed, others have reported that rabbit immunoglobulins purified from the same serum could recognize different nanobodies (Haddad et al., 2016).

Immunoprecipitation

IP was performed essentially as previously described (Vazquez-Pianzola et al., 2011): 30 µl of protein-G Sepharose beads (Amersham) and 1 ml of embryo extracts were used per IP. Extracts were prepared from 0-20 h-old embryos expressing a Chc::Myc fusion protein under a maternal Tubulin promoter. Extracts from wild-type embryos (OreR) were also prepared as a negative control. For each IP, 1 ml of undiluted cell culture supernatant of monoclonal anti-BicD 1B11, anti-BicD 4C2, or anti-Myc 9E10 antibodies were bound to the beads. For TACC IP, a solution containing 2 µl of polyclonal anti-TACC UT316 antibodies (Kao and Megraw, 2009) diluted in 1 ml of PBS was used to bind to the protein-G beads. Beads were resuspended in 30 µl of sample buffer, and 7-15 µl per well was analyzed by western blot, as described above.

Immunostainings

Immunostainings of embryos were performed using the following primary antibodies: mouse anti-BicD (a mix of 1B11 and 4C2, 1:10), mouse anti-Myc 9E10 (1:5), mouse anti-V5 (1:200, Invitrogen, R960-25), rabbit anti-Cnn [1:500, a gift from T. Kaufman (Indiana University, Bloomington, USA) (Heuer et al., 1995)], rabbit anti-Clc [1:500 (Heerssen et al., 2008)], mouse monoclonal anti-α-tubulin DM1A (1:500, Sigma, T9026 or T6199), rabbit anti-α-tubulin (1:500, Abcam, ab18251), guinea pig anti-α-tubulin (1:1000, Geneva Antibody Facility, AA345), rabbit anti-GFP (1:300, previously preabsorbed on embryos), rabbit anti-D-TACC UT316 [1:1000, a gift from T. Megraw (Kao and Megraw, 2009)], rabbit anti-D-TACC [1:500 (Gergely et al., 2000)], mouse anti-D-TACC [1:200, a gift from D. Van Vactor (Blavatnik Institute, Harvard Medical School, Boston, MA, USA) (Chou et al., 2020)], rabbit anti-Pav [1:200, a gift from K. Haglund (Oslo University Hospital, Norway) (Lie-Jensen et al., 2019)], rabbit anti-Asp [1:250, a gift from G. Goshima (Nagoya University, Japan) (Ito and Goshima, 2015)], rabbit anti-Msps [1:500, a gift from H. Ohkura (University of Edinburgh, UK) (Cullen et al., 1999)], mouse anti-Flag M2 (1:200, Sigma, F3165), rabbit anti-CID [1:400, a gift from G. C. Rogers (Arizona Cancer Center, University of Arizona, Tucson, USA) (Buster et al., 2013)], rabbit anti-p-Histone H3 (S10) (1:200, Cell Signaling Technology, 9701L), mouse anti-p-Histone H3 6G3 (1:200, Cell Signaling Technology, 9706), rabbit anti-BubR1 [1:2000, a gift from C. E. Sunkel (Universidade do Porto, Portugal) (Logarinho et al., 2004)], rabbit anti-Mad2 [1:1000, a gift from C. E. Sunkel (Logarinho et al., 2004)], rabbit anti-EB1 (1:500, a gift from G. C. Rogers (Rogers et al., 2002)] and rabbit anti-Clip190 [1:50, a gift from K. G. Miller (Washington University, St Louis, MO, USA) (Lantz and Miller, 1998)]. To detect the hb-deGRadFP construct, anti-llama IgG-heavy and light chain antibodies (1:500) were developed using donkey anti-goat Alexa Fluor 680 (H+L) (1:400, Invitrogen, A21084). Secondary antibodies used were Cy3-conjugated goat anti-mouse (1:800, Jackson ImmunoResearch, 115-165-146), Alexa Fluor 647-conjugated goat anti-mouse (1:400, Jackson ImmunoResearch, 115-606-146), DyLight 649-conjugated or anti-rabbit (1:400, Jackson ImmunoResearch, 111-495-144), A488-conjugated goat anti-rabbit (1:400, Molecular Probes, A-11034), Oregon Green 488-conjugated goat anti-mouse (1:800, Invitrogen, O11033), donkey anti-mouse AF488 (1:1000, Life Technologies, A21202), AF568-conjugated donkey anti-mouse (1:1000, Life Technologies, A100037) and AF488-conjugated donkey anti-rabbit A488 (1:500, Molecular Probes, A21206). Nuclei were visualized by staining DNA with 2.5 µg/ml Hoechst 33258 (Molecular Probes) either for 40 min during the final wash or after being incubated overnight when early meiosis in embryos was analyzed. Control immunostainings using only secondary antibodies were performed to detect unspecific binding of the secondary antibodies. For colocalization studies, control samples using only one of the primary antibodies and both secondary antibodies were prepared to detect bleed through to the other channel. When detecting tagged proteins, samples of wild-type specimens were used to control for unspecific binding of the anti-tag antibody. As indicated, embryos were fixed with either 4% paraformaldehyde (PFA) or methanol. Methanol fixation was mainly used to preserve the cytoskeleton structure and reduce the cytoplasmic levels in BicD staining, and was performed as previously described (Kellogg et al., 1988). When antigens were not well preserved in methanol fixations (as observed, for example, for the Chc fusion proteins), fixation with 4% PFA was used. To detect endogenous BicD::GFP in ovaries, ovaries were fixed with 4% PFA. For preserving the endogenous Clc::GFP signal, embryos were devitellinized by hand and fixed in a mixture of heptane saturated with PFA for 15 min. To preserve the Dj:mCherry and Chc::mCherry signals, the embryos were fixed with methanol. S14 oocytes were prepared for immunostainings as previously described (Radford and McKim, 2016).

Images were analyzed with a Leica TCS-SP8 confocal microscope. Most of the spindle images represent *Z*-stack maximal intensity projections along the frames. MII and AII images were acquired such that the central aster signal was highest, but below saturation.

Given the strong Clc signal in the cytoplasm, the position of the spindle perpendicular to the surface and the depth of the sample, it was not possible to analyze Clc localization at the different regions of the meiotic spindles by directly analyzing the *Z*-stack of maximal confocal projection images. The high cytoplasmic signal in the first planes masked the localization at the spindle in the deeper planes. Thus, to detect the presence of Clc along the tandem meiosis spindles, *Z*-stack images were processed in ImageJ to correct for depth and bleaching. All stacks were processed the same way. First, a crop area corresponding to the spindle of the same size was cropped in each image. Channels were then split and subjected to corrections separately. Each channel was smooth with a median filter radius of 1 to decrease the noise. The channel corresponding to the Clc staining had the most robust signal intensity loss through the depth of the sample. This channel was subject to bleach correction with a simple ratio fit to compensate for intensity attenuation in the deeper stacks of the image. Channels corresponding to α-tubulin and DNA staining did not lose much intensity with the depth of the sample. They were subjected to an attenuation correction using an ImageJ plugin already described (Biot et al., 2008). After intensity correction, the final image was created by merging the channels previously subjected to maximal intensity *Z*-stack projection.

Live imaging in *Drosophila* embryos

To analyze the localization of Chc during the cell cycle, embryos expressing the corresponding fluorescent proteins (Chc::mCherry or Chc::GFP) were imaged with the resonance scanner of a Leica Sp8 confocal microscope. To analyze Chc particle movements, Chc::mCherry embryos were imaged with

Development (2022) 149, dev199944. doi:10.1242/dev.199944

a Nikon W1 LIPSI spinning disk microscope. Images were taken every 0.5 s with a 100× immersion objective. Given that the embryos moved during the cell cycle, we analyzed the particle movement during a total of 150 frames corresponding to 75 s. The particles were detected and tracked using the TrackMate plugin in Fiji (Tinevez et al., 2017). The following settings were used: blob diameter, 0.75 mm; threshold, 2; linking maximal distance, 0.75 mm; gap-closing maximal distance, and frame gap, 0.

Fluorescence *in situ* hybridization

Synthesis of RNA probes and hybridization experiments for mRNA FISH were performed as previously described (Vazquez-Pianzola et al., 2017). To detect deGRadFP mRNA, the *VhhGFP4* region of the *hb-deGRadFP* transgene was first amplified by PCR with primers containing T3 and T7 promoter sequences, and using the plasmid pUAS-Nslmb-VhhGFP4 as a template (Caussinus et al., 2011). Primer sequences were as follows: sense primer containing the T3 promoter, GGGGGGAATTAACCCTCACTAAAGGGAGAATGGATCAAGTCCAACTGGTGGAGT; antisense primer containing the T7 promoter, GGGGGGTAATACGACTCACTATAGGGAGATTAGCTGGAGACGGTGACCTGGGTG. Antisense and sense probes were generated using T7 and T3 RNA polymerase, respectively. A sense probe was used to detect unspecific background.

DNA FISH of *Drosophila* chromosomes was performed mainly according to Dernburg (2000). DNA oligos hybridizing to repetitive regions of the Y (AATAC)6 and the second chromosome (AACAC)7 modified with Cy3 and Cy5 fluorophores at their 5′ end, respectively, were ordered from Microsynth. The sequences were as described previously (Dernburg, 2000). The sequence used to detect the X chromosome by hybridizing to TTT-TCC-AAA-TTT-CGG-TCA-TCA-AAT-AAT-CAT recognizes the 359-bp satellite block on the *Drosophila melanogaster* X chromosome as well as minor variants on chromosome 3, and was described by Ferree and Barbash (2009). A 5′-end Cy5 fluorophore-labeled probe was used. Embryos were fixed with methanol for DNA FISH. Probes were used at a final concentration of 5 ng/µl in hybridization buffer. The blocking buffer used (before adding the first antibody for detection of the desired proteins) was: 2× SSC, 0.5% BSA (molecular grade BSA from BioLabs or acetylated BSA from Ambion) and Tween-20 at 0.1%. Donkey fluorescent-conjugated secondary antibodies were used as described in the immunofluorescence experiments above.

Yeast two-hybrid experiments

Drosophila Egalitarian (Egl; CG4051) full-length, Bicaudal-D full-length and carboxy-terminal (CTD; amino acids 535-782) cDNAs were cloned into the pOAD and/or pOBD2 vectors (Cagney et al., 2000) in-frame either with the activator domain (AD) or the DNA-binding domain (BD) sequence of GAL4, respectively, to create the 'prey' plasmids pEgl-AD, pBicD-AD and pBicD-CTD-AD, as well as the 'bait' plasmids pEgl-BD, pBicD-BD and pBicD-CTD-BD. *D-TACC* (CG9765) full-length; and *Chc* (CG9012) full-length, a fragment containing amino acids 329-803, and another bearing amino acids 329-542 were cloned into the pOAD and or pOBD2 vectors (Cagney et al., 2000) in-frame either with the activator domain (AD) or the DNA-binding domain (BD) sequence of GAL4, respectively, to create the 'prey' plasmids, pD-TACC-AD, pChc-AD, pChc (329-803)-AD, and pChc(329-542)-AD, as well as the 'bait' plasmids pChc-BD, pChc (329-803)-BD and pChc (329-542)-BD. To produce the constructs D-TACC-Ala and D-TACC-Asp, D-TACC Ser^{863} was mutated to an alanine and aspartic acid codon, respectively, by site-directed mutagenesis. Changes were verified by sequencing.

TACC was cloned into the vector pYX122 (Westermann et al., 2000; Addgene #45048; a kind gift from Prof. María Soledad Funes, Instituto de Fisiología Celular, UNAM, Mexico), which lacks the GFP reporter cistron, to generate the construct pTACC-YX22, which expresses TACC under the constitutive TPI promoter. pYX122 contains the auxotrophic gene marker *His3*. Interactions between 'bait' and 'prey' proteins were detected following a yeast interaction-mating method using the strains PJ69-4a and PJ69-4alpha (Cagney et al., 2000). For all cases, diploid cells containing both AD and BD constructs were selected in media lacking tryptophan and leucine [−(L,W), growth test]. To test for possible interactions, cells were further replica-plated in media lacking leucine, tryptophan and adenine [−(L,W,a)], media lacking leucine, tryptophan, histidine and adenine [−(L,W,H,a)] or media lacking leucine, tryptophan and histidine, and containing the indicated amounts of 3-amino-1,2,4-triazole (3AT) [−(interaction test)]. To analyze the effect of TACC on the BicD CTD and Chc interaction in the Y2H system, diploid cells containing both bait Chc-BD and prey BicD CTD-AD plasmids were grown on the auxotrophic medium −(L,W), further co-transformed with either a pYX122 empty vector or pTACC-YX22 and plated onto the auxotrophic media −(L,W,H). The interaction was detected in serial dilutions plated onto −(L,W,H,a). Ten-fold serial dilutions are presented for each test. Growth was scored after 4-to-5 days of growth at 30°C.

C. elegans strains, RNAi and imaging

N2, JDU233 (*H2B::mCherry;α-tubulin::GFP*), VJ512, *chc-1(tm2866)III/hT2[bli-4(e937) let-?(q782) qIs48](I;III)* worms were fed with dsRNA on nematode growth media [2.5 g/l peptone, 20 g/l agar, 3 g/l NaCl, 1 mM $CaCl_2$, 1 mM $MgSO_4$, 25 mM KH_2/K_2HPO_4 (pH 6) buffer, 0.005 mg/ml cholesterol] plates containing 1 mM IPTG and carbenicillin using clones from the Ahringer RNAi library (Kamath and Ahringer, 2003). For nonlethal phenotypes, the progeny were imaged after 60 h of feeding of gravid adults at 20°C. For lethal phenotypes, L3/L4 larvae were transferred onto RNAi plates and fed for 12 h at room temperature to obtain gravid adults. The empty vector L4440 was used as a control. Embryo dissections were performed as previously described (Bellanger et al., 2007), and embryos were imaged immediately on an agar pad using a Zeiss AxioVision microscope with a 100× NA 1.4 oil objective with a GFP and a mCherry filter set. One plane was acquired every 10 s using VisiView, and images were processed using ImageJ and Adobe Photoshop.

Satistical analysis

Statistical analysis was performed using Prism9 software. An ordinary one-way ANOVA test was used for multiple comparisons and an unpaired Student's *t*-test was used when two conditions were analyzed.

Acknowledgements

We thank S. Bullock, C. Bazinet, J. Hirst, M. S. Robinson, D. Graeme, T. Kaufman, K. G. Miller, J. Raff, T. Melgraw, H. Ohkura, G. Rogers, C. Sunkel, M. Affolter, E. Caussinus, D. Van Vactor, K. Haglund, G. Goshima, J. Dumont, the Bloomington *Drosophila* Stock Center (NIH P400D018537) and the Developmental Studies Hybridoma Bank (created by the NICHD of the NIH and maintained at The University of Iowa, Department of Biology, Iowa City, IA 52242) for constructs, fly or worms stocks and antibodies. We thank FlyBase (U41HG000739) for the *Drosophila* genomic resources. We thank Andrew Swan for his scientific advice on how to study female meiosis and Yury Belyaev for his help with image processing.

Competing interests

The authors declare no competing or financial interests.

Author contributions

Conceptualization: P.V.-P., P.M., B.S.; Methodology: P.V.-P., G.S., G.H., P.M., B.S., D. Beuchle; Formal analysis: P.V.-P.; Investigation: P.V.-P., D. Beuchle, G.S., G.H., G.M., D. Brunssen; Resources: P.M., B.S.; Writing - original draft: P.V.-P.; Writing - review & editing: P.V.-P., G.S., G.H., P.M., B.S., D. Beuchle; Visualization: P.V.-P., G.S., G.H.; Supervision: P.V.-P., P.M., B.S.; Project administration: P.V.-P., B.S.; Funding acquisition: P.V.-P., P.M., B.S.

Funding

This work was supported by funding from the Schweizerischer Nationalfonds zur Förderung der wissenschaftlichen Forschung (31003A_173188) and the University of Bern to B.S., by a Schweizerischer Nationalfonds zur Förderung der wissenschaftlichen Forschung grant (IZCOZ0_189884/31003A_176226) to P.M., and by an Equal Opportunity grant from the Philosophisch-Naturwissenschaftliche Fakultät of Bern University to P.V.-P.

Peer review history

The peer review history is available online at https://journals.biologists.com/dev/article-lookup/doi/10.1242/dev.199944.

References

Barros, T. P., Kinoshita, K., Hyman, A. A. and Raff, J. W. (2005). Aurora A activates D-TACC-Msps complexes exclusively at centrosomes to stabilize

centrosomal microtubules. *J. Cell. Biol.* **170**, 1039-1046. doi:10.1083/jcb.200504097

Basto, R., Scaerou, F., Mische, S., Wojcik, E., Lefebvre, C., Gomes, R., Hays, T. and Karess, R. (2004). In vivo dynamics of the rough deal checkpoint protein during *Drosophila* mitosis. *Curr. Biol.* **14**, 56-61. doi:10.1016/j.cub.2003.12.025

Bazinet, C., Katzen, A. L., Morgan, M., Mahowald, A. P. and Lemmon, S. K. (1993). The *Drosophila* clathrin heavy chain gene: clathrin function is essential in a multicellular organism. *Genetics* **134**, 1119-1134. doi:10.1093/genetics/134.4.1119

Bellanger, J.-M., Carter, J. C., Phillips, J. B., Canard, C., Bowerman, B. and Gönczy, P. (2007). ZYG-9, TAC-1 and ZYG-8 together ensure correct microtubule function throughout the cell cycle of *C. elegans* embryos. *J. Cell Sci.* **120**, 2963-2973. doi:10.1242/jcs.004812

Berleth, T., Burri, M., Thoma, G., Bopp, D., Richstein, S., Frigerio, G., Noll, M. and Nüsslein-Volhard, C. (1988). The role of localization of *bicoid* RNA in organizing the anterior pattern of the *Drosophila* embryo. *EMBO J.* **7**, 1749-1756. doi:10.1002/j.1460-2075.1988.tb03004.x

Biot, E., Crowell, E., Höfte, H., Maurin, Y., Vernhettes, S. and Andrey, P. (2008). A new filter for spot extraction in N-dimensional biological imaging. In Fifth IEEE International Symposium on Biomedical Imaging (ISBI'08): From Nano to Macro, pp. 975-978.

Booth, D. G., Hood, F. E., Prior, I. A. and Royle, S. J. (2011). A TACC3/ch-TOG/clathrin complex stabilises kinetochore fibres by inter-microtubule bridging. *EMBO J.* **30**, 906-919. doi:10.1038/emboj.2011.15

Brodsky, F. M. (2012). Diversity of clathrin function: new tricks for an old protein. *Annu. Rev. Cell Dev. Biol.* **28**, 309-336. doi:10.1146/annurev-cellbio-101011-155716

Bullock, S. L. and Ish-Horowicz, D. (2001). Conserved signals and machinery for RNA transport in *Drosophila* oogenesis and embryogenesis. *Nature* **414**, 611-616. doi:10.1038/414611a

Buster, D. W., Daniel, S. G., Nguyen, H. Q., Windler, S. L., Skwarek, L. C., Peterson, M., Roberts, M., Meserve, J. H., Hartl, T., Klebba, J. E. et al. (2013). SCFSlimb ubiquitin ligase suppresses condensin II-mediated nuclear reorganization by degrading Cap-H2. *J. Cell Biol.* **201**, 49-63. doi:10.1083/jcb.201207183

Cagney, G., Uetz, P. and Fields, S. (2000). High-throughput screening for protein-protein interactions using two-hybrid assay. *Meth. Enzymol.* **328**, 3-14. doi:10.1016/S0076-6879(00)28386-9

Caussinus, E., Kanca, O. and Affolter, M. (2011). Fluorescent fusion protein knockout mediated by anti-GFP nanobody. *Nat. Struct. Mol. Biol.* **19**, 117-121. doi:10.1038/nsmb.2180

Chou, V. T., Johnson, S., Long, J., Vounatsos, M. and van Vactor, D. (2020). dTACC restricts bouton addition and regulates microtubule organization at the Drosophila neuromuscular junction. *Cytoskeleton (Hoboken)* **77**, 4-15. doi:10.1002/cm.21578

Cullen, C. F., Deák, P., Glover, D. M. and Ohkura, H. (1999). *mini spindles*: a gene encoding a conserved microtubule-associated protein required for the integrity of the mitotic spindle in *Drosophila*. *J. Cell Biol.* **146**, 1005-1018. doi:10.1083/jcb.146.5.1005

Défachelles, L., Hainline, S. G., Menant, A., Lee, L. A. and Karess, R. E. (2015). A maternal effect *rough deal* mutation suggests that multiple pathways regulate *Drosophila* RZZ kinetochore recruitment. *J. Cell Sci.* **128**, 1204-1216. doi:10.1242/jcs.176826

Dernburg, A. F. (2000). *In Situ* hybridization to somatic chromosomes. In *Drosophila Protocols* (ed. W. Sullivan, M. Ashburner and R. S. Hawley), pp. 24-55. Cold Spring Harbor, New York, USA: Cold Spring Harbor Laboratory Press.

Dienstbier, M., Boehl, F., Li, X. and Bullock, S. L. (2009). Egalitarian is a selective RNA-binding protein linking mRNA localization signals to the dynein motor. *Genes Dev.* **23**, 1546-1558. doi:10.1101/gad.531009

Driever, W. and Nüsslein-Volhard, C. (1988). A gradient of bicoid protein in *Drosophila* embryos. *Cell* **54**, 83-93. doi:10.1016/0092-8674(88)90182-1

Ferree, P. M. and Barbash, D. A. (2009). Species-specific heterochromatin prevents mitotic chromosome segregation to cause hybrid lethality in *Drosophila*. *PLoS Biol.* **7**, e1000234. doi:10.1371/journal.pbio.1000234

Fischer, M. G., Heeger, S., Häcker, U. and Lehner, C. F. (2004). The mitotic arrest in response to hypoxia and of polar bodies during early embryogenesis requires *Drosophila Mps1*. *Curr. Biol.* **14**, 2019-2024.

Fu, W., Tao, W., Zheng, P., Fu, J., Bian, M., Jiang, Q., Clarke, P. R. and Zhang, C. (2010). Clathrin recruits phosphorylated TACC3 to spindle poles for bipolar spindle assembly and chromosome alignment. *J. Cell Sci.* **123**, 3645-3651. doi:10.1242/jcs.075911

Fumoto, K., Hoogenraad, C. C. and Kikuchi, A. (2006). GSK-3beta-regulated interaction of BICD with dynein is involved in microtubule anchorage at centrosome. *EMBO J.* **25**, 5670-5682. doi:10.1038/sj.emboj.7601459

Gergely, F., Kidd, D., Jeffers, K., Wakefield, J. G. and Raff, J. W. (2000). D-TACC: a novel centrosomal protein required for normal spindle function in the early *Drosophila* embryo. *EMBO J.* **19**, 241-252. doi:10.1093/emboj/19.2.241

Gönczy, P., Pichler, S., Kirkham, M. and Hyman, A. A. (1999). Cytoplasmic dynein is required for distinct aspects of MTOC positioning, including centrosome separation, in the one cell stage *Caenorhabditis elegans* embryo. *J. Cell Biol.* **147**, 135-150. doi:10.1083/jcb.147.1.135

Griffis, E. R., Stuurman, N. and Vale, R. D. (2007). Spindly, a novel protein essential for silencing the spindle assembly checkpoint, recruits dynein to the kinetochore. *J. Cell Biol.* **17**, 1005-1015. doi:10.1083/jcb.200702062

Gutierrez-Caballero, C., Burgess, S. G., Bayliss, R. and Royle, S. J. (2015). GTACC3-ch-TOG track the growing tips of microtubules independently of clathrin and Aurora-A phosphorylation. *Biol. Open* **4**, 170-179. doi:10.1242/bio.201410843

Haddad, M., Soukkarieh, C., Khalaf, H. E. and Abbady, A. Q. (2016). Purification of polyclonal IgG specific for Camelid's antibodies and their recombinant nanobodies. *Open Life Sci.* **11**, 1-9. doi:10.1515/biol-2016-0001

Heerssen, H., Fetter, R. D. and Davis, G. W. (2008). Clathrin dependence of synaptic-vesicle formation at the *Drosophila* neuromuscular junction. *Curr. Biol.* **18**, 401-409. doi:10.1016/j.cub.2008.02.055

Heuer, J. G., Li, K. and Kaufman, T. C. (1995). The *Drosophila* homeotic target gene *centrosomin (cnn)* encodes a novel centrosomal protein with leucine zippers and maps to a genomic region required for midgut morphogenesis. *Development* **121**, 3861-3876. doi:10.1242/dev.121.11.3861

Hirst, J., Sahlender, D. A., Choma, M., Sinka, R., Harbour, M. E., Parkinson, M. and Robinson, M. S. (2009). Spatial and functional relationship of GGAs and AP-1 in Drosophila and HeLa cells. *Traffic* **10**, 1696-1710. doi:10.1111/j.1600-0854.2009.00983.x

Hood, F. E., Williams, S. J., Burgess, S. G., Richards, M. W., Roth, D., Straube, A., Pfuhl, M., Bayliss, R. and Royle, S. J. (2013). Coordination of adjacent domains mediates TACC3–ch-TOG–clathrin assembly and mitotic spindle binding. *J. Cell Biol.* **202**, 463-478. doi:10.1083/jcb.201211127

Hoogenraad, C. C. and Akhmanova, A. (2016). Bicaudal D family of motor adaptors: linking dynein motility to cargo binding. *Trends Cell Biol.* **26**, 327-340. doi:10.1016/j.tcb.2016.01.001

Howell, B. J., McEwen, B. F., Canman, J. C., Hoffman, D. B., Farrar, E. M., Rieder, C. L. and Salmon, E. D. (2001). Cytoplasmic dynein/dynactin drives kinetochore protein transport to the spindle poles and has a role in mitotic spindle checkpoint inactivation. *J. Cell Biol.* **155**, 1159-1172. doi:10.1083/jcb.200105093

Ito, A. and Goshima, G. (2015). Microcephaly protein Asp focuses the minus ends of spindle microtubules at the pole and within the spindle. *J. Cell Biol.* **211**, 999-1009. doi:10.1083/jcb.201507001

Kamath, R. S. and Ahringer, J. (2003). Genome-wide RNAi screening in Caenorhabditis elegans. *Methods* **30**, 313-321. doi:10.1016/S1046-2023(03)00050-1

Kao, L.-R. and Megraw, T. L. (2009). Centrocortin cooperates with centrosomin to organize *Drosophila* embryonic cleavage furrows. *Curr. Biol.* **19**, 937-942. doi:10.1016/j.cub.2009.04.037

Kasprowicz, J., Kuenen, S., Miskiewicz, K., Habets, R. L. P., Smitz, L. and Verstreken, P. (2008). Inactivation of clathrin heavy chain inhibits synaptic recycling but allows bulk membrane uptake. *J. Cell Biol.* **182**, 1007-1016. doi:10.1083/jcb.200804162

Kellogg, D. R., Mitchison, T. J. and Alberts, B. M. (1988). Behaviour of microtubules and actin filaments in living *Drosophila* embryos. *Development* **103**, 675-686. doi:10.1242/dev.103.4.675

Koch, R., Ledermann, R., Urwyler, O., Heller, M. and Suter, B. (2009). Systematic functional analysis of Bicaudal-D serine phosphorylation and intragenic suppression of a female sterile allele of *BicD*. *PLoS ONE* **4**, e4552. doi:10.1371/journal.pone.0004552

Lantz, V. A. and Miller, K. G. (1998). A class VI unconventional myosin is associated with a homologue of a microtubule-binding protein, cytoplasmic linker protein-170, in neurons and at the posterior pole of Drosophila embryos. *J. Cell Biol.* **140**, 897-910. doi:10.1083/jcb.140.4.897

Lee, M. J., Gergely, F., Jeffers, K. Peak-Chew, S. Y. and Raff, J. W. (2001). Msps/XMAP215 interacts with the centrosomal protein D-TACC to regulate microtubule behaviour. *Nat. Cell Biol* **3**, 643-649. doi:10.1038/35083033

Li, X., Kuromi, H., Briggs, L., Green, D. B., Rocha, J. J., Sweeney, S. T. and Bullock, S. L. (2010). Bicaudal-D binds clathrin heavy chain to promote its transport and augments synaptic vesicle recycling. *EMBO J.* **29**, 992-1006. doi:10.1038/emboj.2009.410

Lie-Jensen, A., Ivanauskiene, K., Malerød, L., Jain, A., Tan, K. W., Laerdahl, J. K., Liestøl, K., Stenmark, H. and Haglund, K. (2019). Centralspindlin recruits ALIX to the midbody during cytokinetic abscission in Drosophila via a mechanism analogous to virus budding. *Curr. Biol.* **29**, 3538-3548.e7. doi:10.1016/j.cub.2019.09.025

Lin, C.-H., Hu, C.-K. and Shih, H.-M. (2010). Clathrin heavy chain mediates TACC3 targeting to mitotic spindles to ensure spindle stability. *J. Cell Biol.* **189**, 1097-1105. doi:10.1083/jcb.200911120

Logarinho, E., Bousbaa, H., Dias, J. M., Lopes, C., Amorim, I., Antunes-Martins, A. and Sunkel, C. E. (2004). Different spindle checkpoint proteins monitor microtubule attachment and tension at kinetochores in *Drosophila* cells. *J. Cell Sci.* **117**, 1757-1771. doi:10.1242/jcs.01033

Lucaj, C. M., Evans, M. F., Nwagbara, B. U., Ebbert, P. T., Baker, C. C., Volk, J. G., Francl, A. F., Ruvolo, S. P. and Lowery, L. A. (2015). *Xenopus* TACC1 is a microtubule plus-end tracking protein that can regulate microtubule dynamics

during embryonic development. *Cytoskeleton* **72**, 225-234. doi:10.1002/cm.21224

Mach, J. M. and Lehmann, R. (1997). An Egalitarian-BicaudalD complex is essential for oocyte specification and axis determination in *Drosophila*. *Genes Dev.* **11**, 423-435. doi:10.1101/gad.11.4.423

Margolis, J. S., Borowsky, M., Shim, C. W. and Posakony, J. W. (1994). A small region surrounding the distal promoter of the *hunchback* gene directs maternal expression. *Dev. Biol.* **163**, 381-388. doi:10.1006/dbio.1994.1156

Nag, R. N., Niggli, S., Sousa-Guimarães, S., Vazquez-Pianzola, P. and Suter, B. (2018). *Mms19* is a mitotic gene that permits Cdk7 to be fully active as a Cdk-activating kinase. *Development* **145**, dev156802. doi:10.1242/dev.156802

Nwagbara, B. U, Faris, A. E., Bearce, E. A., Erdogan, B. and Ebbert, P. T. (2014). TACC3 is a microtubule plus end-tracking protein that promotes axon elongation and also regulates microtubule plus end dynamics in multiple embryonic cell types. *Mol. Biol. Cell* **25**, 3350-3362. doi:10.1091/mbc.E14-06-1121

Paré, C. and Suter, B. (2000). Subcellular localization of Bic-D::GFP is linked to an asymmetric oocyte nucleus. *J. Cell Sci.* **113**, 2119-2127. doi:10.1242/jcs.113.12.2119

Payne, C., Rawe, V., Ramalho-Santos, J., Simerly, C. and Schatten, G. (2003). Preferentially localized dynein and perinuclear dynactin associate with nuclear pore complex proteins to mediate genomic union during mammalian fertilization. *J. Cell Sci.* **116**, 4727-4738. doi:10.1242/jcs.00784

Pérez-Mongiovi, D., Malmanche, N., Bousbaa, H. and Sunkel, C. (2005). Maternal expression of the checkpoint protein BubR1 is required for synchrony of syncytial nuclear divisions and polar body arrest in *Drosophila melanogaster*. *Development* **132**, 4509-4520. doi:10.1242/dev.02028

Raaijmakers, J. A. and Medema, R. H. (2014). Function and regulation of dynein in mitotic chromosome segregation. *Chromosoma* **123**, 407-422. doi:10.1007/s00412-014-0468-7

Radford, S. J. and McKim, K. S. (2016). Techniques for imaging prometaphase and metaphase of meiosis i in fixed *Drosophila* oocytes. *J. Vis. Exp.* **116**, e54666. doi:10.3791/54666

Ran, B., Bopp, R. and Suter, B. (1994). Null alleles reveal novel requirements for *Bic-D* during *Drosophila* oogenesis and zygotic development. *Development* **120**, 1233-1242. doi:10.1242/dev.120.5.1233

Rieder, C. L. and Maiato, H. (2004). Stuck in division or passing through: what happens when cells cannot satisfy the spindle assembly checkpoint. *Dev. Cell* **7**, 637-651. doi:10.1016/j.devcel.2004.09.002

Rogers, S. L. , Rogers, G. C., Sharp, D. J. and Vale, R. D. (2002). Drosophila EB1 is important for proper assembly, dynamics, and positioning of the mitotic spindle. *J. Cell. Biol.* **158**, 873-884. doi:10.1083/jcb.200202032

Royle, S. J. (2012). The role of clathrin in mitotic spindle organisation. *J. Cell Sci.* **125**, 19-28. doi:10.1242/jcs.094607

Royle, S. J. and Lagnado, L. (2006). Trimerisation is important for the function of clathrin at the mitotic spindle. *J. Cell Sci.* **119**, 4071-4078. doi:10.1242/jcs.03192

Royle, S. J., Bright, N. A. and Lagnado, L. (2005). Clathrin is required for the function of the mitotic spindle. *Nature* **434**, 1152-1157. doi:10.1038/nature03502

Rutherford, E. L., Carandang, L., Ebbert, P. T., Mills, A. N., Bowers, J. T. and Lowery, L. A. (2016). Xenopus TACC2 is a microtubule plus end-tracking protein that can promote microtubule polymerization during embryonic development. *Mol. Biol. Cell* **27**, 3013-3020. doi:10.1091/mbc.E16-03-0198

Sallés, F. J., Lieberfarb, M. E., Wreden, C., Gergen, J. P. and Strickland, S. (1994). Coordinate initiation of *Drosophila* development by regulated polyadenylation of maternal messenger RNAs. *Science* **266**, 1996-1999. doi:10.1126/science.7801127

Sawicka, A. and Seiser, C. (2012). Histone H3 phosphorylation - a versatile chromatin modification for different occasions. *Biochimie* **94**, 2193-2201. doi:10.1016/j.biochi.2012.04.018

Schulz, C. and Tautz, D. (1995). Zygotic *caudal* regulation by *hunchback* and its role in abdominal segment formation of the *Drosophila* embryo. *Development* **121**, 1023-1028. doi:10.1242/dev.121.4.1023

So, C., Seres, K. B., Steyer, A. M., Mönnich, E., Clift, D., Pejkovska, A., Möbius, W. and Schuh, M. (2019). A liquid-like spindle domain promotes acentrosomal spindle assembly in mammalian oocytes. *Science* **364**, eaat9557. doi:10.1126/science.aat9557

Sokac, A. M. and Wieschaus, E. (2008). Local actin-dependent endocytosis is zygotically controlled to initiate *Drosophila* cellularization. *Dev. Cell* **14**, 775-786. doi:10.1016/j.devcel.2008.02.014

Splinter, D., Razafsky, D. S., Schlager, M. A., Serra-Marques, A., Grigoriev, I., Demmers, J., Keijzer, N., Jiang, K., Poser, I., Hyman, A. A. et al. (2012). BICD2, dynactin, and LIS1 cooperate in regulating dynein recruitment to cellular structures. *Mol. Biol. Cell* **23**, 4226-4241. doi:10.1091/mbc.e12-03-0210

Suter, B. and Steward, R. (1991). Requirement for phosphorylation and localization of the Bicaudal-D protein in *Drosophila* oocyte differentiation. *Cell* **67**, 917-926. doi:10.1016/0092-8674(91)90365-6

Suter, B., Romberg, L. M. and Steward, R. (1989). *Bicaudal-D*, a *Drosophila* gene involved in developmental asymmetry: localized transcript accumulation in ovaries and sequence similarity to myosin heavy chain tail domains. *Genes Dev.* **3**, 1957-1968. doi:10.1101/gad.3.12a.1957

Swan, A. and Suter, B. (1996). Role of *Bicaudal-D* in patterning the *Drosophila* egg chamber in mid-oogenesis. *Development* **122**, 3577-3586. doi:10.1242/dev.122.11.3577

Tinevez, J.-Y., Perry, N., Schindelin, J., Hoopes, G. M., Reynolds, G. D., Laplantine, E., Bednarek, S. Y., Shorte, S. L. and Eliceiri, K. W. (2017). TrackMate: an open and extensible platform for single-particle tracking. *Methods* **115**, 80-90. doi:10.1016/j.ymeth.2016.09.016

Vazquez-Pianzola, P. and Suter, B. (2012). Conservation of the RNA transport machineries and their coupling to translation control across eukaryotes. *Comp. Funct. Genomics* **2012**, 287852. doi:10.1155/2012/287852

Vazquez-Pianzola, P., Urlaub, H. and Suter, B. (2011). Pabp binds to the *osk* 3′ UTR and specifically contributes to *osk* mRNA stability and oocyte accumulation. *Dev. Biol.* **357**, 404-418. doi:10.1016/j.ydbio.2011.07.009

Vazquez-Pianzola, P., Adam, J., Haldemann, D., Hain, D., Urlaub, H. and Suter, B. (2014). Clathrin heavy chain plays multiple roles in polarizing the *Drosophila* oocyte downstream of *Bic-D*. *Development* **141**, 1915-1926. doi:10.1242/dev.099432

Vazquez-Pianzola, P., Suter, B. and Hernández, G. (2016). Evolution of the molecules coupling mRNA transport with translational control in metazoans. In *Evolution of the Protein Synthesis Machinery and Its Regulation* (ed. G. Hernández and R. Jagus), pp. 531-546. Springer: New York.

Vazquez-Pianzola, P., Schaller, B., Colombo, M., Beuchle, D., Neuenschwander, S., Marcil, A., Bruggmann, R. and Suter, B. (2017). The mRNA transportome of the BicD/Egl transport machinery. *RNA Biol.* **14**, 73-89. doi:10.1080/15476286.2016.1251542

Westermann, B. and Neupert, W. (2000). Mitochondria-targeted green fluorescent proteins: convenient tools for the study of organelle biogenesis in *Saccharomyces cerevisiae*. *Yeast* **16**, 1421-1427. doi:10.1002/1097-0061(200011)16:15<1421::AID-YEA624>3.0.CO;2-U

Wharton, R. P. and Struhl, G. (1989). Structure of the *Drosophila* BicaudalD protein and its role in localizing the posterior determinant *nanos*. *Cell* **59**, 881-892. doi:10.1016/0092-8674(89)90611-9

Wojcik, E., Basto, R., Serr, M., Scaërou, F., Karess, R. and Hays, T. (2001). Kinetochore dynein: its dynamics and role in the transport of the Rough deal checkpoint protein. *Nat. Cell Biol.* **3**, 1001-1007. doi:10.1038/ncb1101-1001